DOE/PC/94055--T2

TECHNOLOGY DEVELOPMENT FOR IRON FISCHER-TROPSCH CATALYSIS

Contract No. DE-AC22-91PC94055

Quarterly Technical Progress Report No. 2

Covering the Period January 1, 1995 to March 31, 1995

Prepared for

U.S. Department of Energy
Pittsburgh Energy Technology Center
PETC Project manager: Richard E. Tischer
P. O. Box 10940
Pittsburgh, PA 15236-0940

Submitted by

Project Manager: Burtron H. Davis
University of Kentucky Research Foundation
Kinkead Hall
Lexington, KY 40506-0057

Date Prepared
May 2, 1995

DISCLAIMER

Portions of this document may be illegible in electronic image products. Images are produced from the best available original document.

2. Contract Objectives

The objective of this research project is to develop the technology for the production of physically robust iron-based Fischer-Tropsch catalysts that have suitable activity, selectivity and stability to be used in the slurry phase synthesis reactor development. The catalysts that are developed shall be suitable for testing in the Advanced Fuels Development Facility at LaPorte, Texas, to produce either low- or high-alpha product distributions. Previous work by the offeror has produced a catalyst formulation that is 1.5 times as active as the "standard-catalyst" developed by German workers for slurry phase synthesis. The proposed work will optimize the catalyst composition and pretreatment operation for this low-alpha catalyst. In parallel, work will be conducted to design a high-alpha iron catalyst this is suitable for slurry phase synthesis. Studies will be conducted to define the chemical phases present at various stages of the pretreatment and synthesis stages and to define the course of these changes. The oxidation/reduction cycles that are anticipated to occur in large, commercial reactors will be studied at the laboratory scale. Catalyst performance will be determined for catalysts synthesized in this program for activity, selectivity and aging characteristics.

The research is divided into four major topical areas: (a) catalyst preparation and characterization, (b) product characterization, (c) reactor operations, and (d) data assessment.

To accomplish the objectives of the project, these topics have been organized into the following technical tasks:

a. Task 1.0 Development of Optimum Promoter Levels for Low- and High-Alpha Catalysts

1.1 Determine Optimized Synthesis Procedure for High-Alpha Iron-Based Fischer-Tropsch Catalysts

- Role of precursor particle size on activity.
- Role of Cu in precipitated catalysts.
- Define attrition resistance.

1.2 Prepare Catalysts that can be Used to Determine the Role of Promoters for Low- and High-Alpha Catalysts

- Define optimum SiO_2.
- Define optimum Al_2O_3.

1.3 Prepare Catalysts that can be Used to Quantify the Role of K on Product Selectivity in both Low- and High-Alpha Catalysts.

1.4 Complete the Optimization of the Two Best Low-Alpha, Iron-Based Fischer-Tropsch Catalysts Developed during the Previous Contract.

b. Task 2.0 Definition of Preferred Pretreatment for both Low- and High-Alpha Fischer-Tropsch Catalysts.

2.1 Determine the Role of Cu in the Activation of Precipitated Low- and High-Alpha, Iron-Based Fischer-Tropsch Catalysts.

2.2 Determine the Effect of K Content on Activation Procedures and Determine if the Method of Addition has any Effect on Catalyst Activity and Life.

2.3 Determine the Physical and Chemical Changes that Occur during Catalyst Pretreatment and Use and Determine how these Changes Effect the Strength of the Catalysts.

2.4 Evaluate the Effect of Carbon Deposition during Catalyst Activation on Activity, Selectivity and Aging Characteristics.

c. Task 3.0 Catalyst Structure and Characterization.

d. Task 4.0 Catalyst Testing.

4.1 Verify the Quality of Data Obtained from the CSTR's.

4.2 Measure Catalyst Performance.

4.3 Determine the Stable Phases that Exist during Synthesis at Low and High CO Conversion Levels.

4.4 Obtain Data on the Rates Involved in the Interconversion of Iron Oxide and Iron Carbide.

e. Task 5.0 Reports.

3. Summary of Activities

The Fischer-Tropsch synthesis has been studied over the best low-alpha catalyst developed at the CAER. A wide range of synthesis gas conversions were obtained by varying the space velocity. The experimental results show that: (i) the rate of the water gas shift reaction is lower than the rate of the Fischer-Tropsch reaction at low conversions (< 60%) whereas it closely approaches the rate of the Fischer-Tropsch synthesis at high conversions, (ii) the fraction of CO converted to hydrocarbons is higher at low and intermediate conversions whereas it is smaller at high conversions, (iii) the H_2/CO ratio of the product gas is equal to the H_2/CO ratio of the inlet synthesis gas at an intermediate

conversion level of 67%. These findings suggest that it would be beneficial to carry out the reaction at intermediate conversions. This would result in an optimum use of CO to produce hydrocarbons rather than CO_2. High overall conversions can be obtained by either using a second reactor or recycling the product gas using a single reactor. If the intermediate conversion in a single pass is maintained at 67% there would be no need to adjust the H_2/CO ratio of the recycle stream or the feed to the second reactor as the product gas from a single pass would have the same H_2/CO ratio as the feed synthesis gas.

The optimum reaction rate expression for synthesis gas conversion has been developed for this catalyst:

$$-r_{CO+H_2} = k\, P_{CO}\, P_{H_2} / (1 + K_{CO} P_{CO})$$

The rate expression shows that CO is strongly adsorbed on the catalyst and that the reaction products such as water and CO_2 do not inhibit the reaction rate.

4. Status, Accomplishments, Results and Discussion

A.0. - Task 1.0. Development of Optimum Promoter Levels for Low- and High-Alpha Catalysts

The goal of this task is to identify and optimize procedure for the preparation of iron-based catalysts that combine high activity selectivity and life with physical robustness. Each of the subtasks address an area of considerable uncertainty in the synthesis of catalysts.

A.1. Determine Optimized Synthesis Procedure for High-Alpha Iron-Based Catalysts

- Role of precursor size on activity.

No scheduled or additional activity to report.

- Role of Cu in precipitated catalysts.

  See Task B.1.

- Define attrition resistance.

  The powder sample of RJO-181 (30 wt.% Fe_2O_3/SiO_2) was used for microhardness test. Cold molds using epoxy hardeners were used to prepare the specimens. After imbedding the particles in the epoxy, they were allowed to harden. Then the epoxy molds were polished. Several particles were photographed in the optical microscope. Using a MICROMET-4 hardness tester, the microhardness measurements were made. The specimen was mounted onto the hardness tester, and a load of 25 gm was used to make the Vicker's indentation on the particles, which are 10 to 50 microns in size. The indentations were so large that they covered the entire particles. Hence, a load of 10 gm (the minimum load available) was used to make the indentations on several individual particles embedded in the epoxy mold. After making the indentations the specimen was mounted on the optical microscope and the diagonal distances of the indentations were measured. The average value of about 50 indentations was taken for measuring the Vicker's hardness, which was calculated to be 40 kg/mm^2. According to the ASTM standards, this number indicates that the material under investigation is very soft. The value of 40 is not accurate, as the hard epoxy under the particles can also take part of the load. This introduces additional uncertainty to the calculated value. For comparison,

the hardness values for several materials are plotted in Figure 1. It can therefore be concluded that the iron oxide catalyst particles are very soft.

A.2. Prepare Catalysts that can be Used to Determine the Role of Promoters for Low- and High-Alpha Catalysts

- Define Optimum SiO_2

  No scheduled or further activity to report.

- Define Optimum Al_2O_3

  No scheduled or further activity to report.

A.3. Prepare Catalysts that can be Used to Quantify the Role of K on Product Selectivity for both High- and Low-Alpha Catalysts

The initial data suggest that a potassium content of 3 wt.% is the optimum concentration for the high-alpha catalysts.

A.4. Complete the Optimization of Two Best Low-Alpha, Iron-Based Catalysts Developed During the Previous Contract

No scheduled or additional activity to report.

A.5. Schedule of Activities for Next Quarter

- Continue efforts to examine the approaches to prepare 400 to 1000 micron spherical particles.
- Continue to evaluate Fe supported on Al_2O_3 for activity.
- Determine the microhardness of the fused, reduced and carbide C-73 catalyst.

B.0. - Task 2.0. Definition of Preferred Pretreatment for Both Low- and High-Alpha Catalysts

The goals of this task are to define the preferred treatment, to define the role of Cu and K during the pretreatment on activity and selectivity and to define the chemical and physical changes which occur during the preferred pretreatment. The subtasks address each of these goals.

B.1. Role of Cu in the Activation of Precipitated Low- and High-Alpha, Iron Based Fischer-Tropsch Catalysts

Syngas activation was carried out on catalysts with the following compositions in atomic % relative to iron: 100Fe/3.6Si/0.71K and 100Fe/3.6Si/2.6Cu/0.71K. Catalysts were loaded into a 1 L CSTR and mixed with a C_{30} oil to give a 10 wt % catalyst slurry. The reactor was pressurized to 13 atm under a flow of syngas (H2/CO=0.7, 3.1 NL h^{-1} g^{-1}(Fe)) and then heated to 270°C at 2°C/min. These conditions were maintained throughout the runs. A comparison of syngas conversion for the two runs is shown in Figure 2. The 100Fe/3.6Si/0.71K catalyst was inactive and had a total syngas conversion of only 18% after 92 hr on stream. Promotion with Cu increased the activity of the catalyst considerably. The syngas conversion for the 100Fe/3.6Si/2.6Cu/0.71K catalyst increased throughout the run and finally reached 50% before the reactor was shutdown due to loss of reactor solvent. X-ray diffraction shows that the 100Fe/3.6Si/0.71K catalyst was composed of Fe_3O_4 while the more active 100Fe/3.6Si/2.6Cu/0.71K catalyst was composed of a mixture of Fe_3O_4 and the carbides: χ-Fe_5C_2 and ϵ'-$Fe_{2.2}C$ (Figure 3). Mössbauer spectroscopy also shows that the 100Fe/3.6Si/0.71K catalyst was composed of only Fe_3O_4 during the run. Mössbauer spectroscopy results for the

100Fe/3.6Si/2.6Cu/0.71K catalyst are shown in Figure 4. In general, the Cu promoted catalyst was composed of approximately 76% Fe_3O_4, 4% of some superparamagnetic component and 20% ϵ'-$Fe_{2.2}C$. These results are consistent with published results that Cu facilitates the reduction of iron oxide to an active state.

Future work with Cu promotion will be focused on its affect on the kinetics of the Fischer-Tropsch Synthesis and on the activity of catalysts operating in a high alpha mode. Previous work has shown that promotion with Cu has little affect on the activity or selectivity of the 100Fe/3.6Si/0.71K catalyst when pretreated with CO at 13 atm and 270°C followed by FTS conducted at 13 atm, 270°C with $H_2/CO=0.7$ (3.1 NL h^{-1} g^{-1}(Fe)). However, under these conditions the CO conversion is very high (>90%) and the true promotional benefits of Cu might not be evident. Decreasing the CO conversion of the catalyst by operating at higher space velocities might give a better indication of the affect Cu has on the activity of iron FTS catalysts. In addition, the affect of Cu on H_2 activation needs to be explored.

B.2. Determine the Effect of K Content on Activation Procedures and Determinate if the Method of Addition has any Effect on Catalyst Activity and Life.

No scheduled or additional activity to report.

B.3. Physical and Chemical Changes that Occur During Pretreatment and Use

The affect of temperature (270°C or 300°C), pressure (13 atm or 1 atm) and gas composition ($H_2/CO=0.7$, 0.1 or 0) on the activation of precipitated iron catalysts with the compositions 100Fe/3.6Si/0.71K and 100Fe/4.4Si/1.0K was studied. In general, it was found that activation with $H_2/CO=0.7$ at 13 atm resulted in poorly active catalysts (CO conversion <20%) when activated at either 270°C or 300°C (Figure 5). Decreasing the

H_2/CO ratio to 0.1 and activating at 13 atm and 270°C resulted in an activity intermediate between activation in pure CO or H_2/CO=0.7 (Figure 6). This suggested that when activating iron catalysts with syngas it is desirable to have a low partial pressure of H_2. In fact, when the catalysts are activated with synthesis gas (H_2/CO=0.7) at 1 atm, 270°C or 300°C conversions comparable to activation with CO are obtained (Figures 7 and 8). No pressure affect was seen when the 100Fe/4.4Si/1.0K catalyst was activated with CO at 270°C and 13 atm or 1 atm (Figure 9). X-ray diffraction analysis of the catalysts following activation show that catalysts with low activity (those activated with syngas at 13 atm) are composed of only Fe_3O_4 while those with high activity (those activated with syngas at 1 atm or CO) are composed of a mixture of Fe_3O_4, χ-Fe_5C_2 and ϵ'-$Fe_{2.2}C$ (Figure 10). These results and the results mentioned above in Task 2.1 (B.1.) indicate that the formation of some iron carbide is necessary for high FTS activity. However, based on previous Mössbauer spectroscopy experiments, we know that the activity of iron catalysts is not related to the amount of iron carbide present. These results tend to indicate that a surface carbide is the active phase.

The influence of H_2 partial pressure on syngas activation can be explained as follows. Based on XRD and Mössbauer spectroscopy results we know that CO or syngas pretreatment of precipitated iron catalysts will rapidly reduce the catalyst to Fe_3O_4. According to the competition model proposed by Niemantsverdriet, surface carbon from dissociated CO can then do three things: become a carbonaceous layer, migrate into the bulk of the catalyst to form iron carbide or be hydrogenated to methyl or methylene groups which participate in the FTS. When an iron catalyst is activated with CO the surface carbon can only become a carbonaceous layer or form a carbide which is

presumed to be necessary for high FTS activity. In the case of syngas activation, H_2 is also present so hydrogenation of the surface carbon can take place. This causes a competition between carbide formation and hydrogenation. At high H_2 partial pressures the hydrogenation of the surface carbon occurs faster than carbide formation so only relatively inactive Fe_3O_4 is formed.

Future work will focus on obtaining Mössbauer data for the catalysts activated with syngas at 1 atm to see if the catalyst compositions are similar to those obtained for CO activation. In addition, characterization of the 100Fe/4.4Si/1.0K catalyst activated with H_2 will be done.

B.4. Effect of Carbon Deposition

Iron catalysts that have high FTS activity contain bulk iron carbide and large amounts of excess carbon. Pretreatment of the 100Fe/3.6Si/0.71K catalyst with CO at 270°C and 13 atm for 24 hr yields a highly active catalyst and yet produces about twice as much carbon as needed for the formation of Fe_5C_2. It is of interest to determine the role of this carbon in the FTS and determine its morphology.

The 100Fe/3.6Si/0.71K catalyst was subjected to syngas (H_2/CO=0.7) activation at 270°C and 13 atm. After 93 hr of synthesis, during which the CO conversion never rose above 12%, H_2 flow was stopped and the catalyst was treated with CO for 22 h. Following the CO treatment the synthesis was restarted. As can be seen in Figure 11, the CO conversion rose very rapidly and reached the same level as when the catalyst is initially activated with CO. X-ray diffraction analysis of catalyst samples withdrawn before and after treating the catalyst with CO show that syngas activation converted the catalyst to Fe_3O_4 and the CO treatment partially reduced the Fe_3O_4 to χ-Fe_5C_2 and ϵ'-$Fe_{2.2}C$.

Mössbauer spectroscopy results showing the phase transformation is shown in Figure 12. Catalyst samples from this run were submitted to Sandia for high-resolution TEM analysis. High resolution TEM of this catalyst series offers the possibility of showing the location of the iron carbide in relation to the Fe_3O_4 and the structure of the free carbon which forms from CO activation.

B.5. Schedule of Activities for Next Quarter

- Begin to define the optimum pretreatment for high-alpha catalysts with emphasis on CO + H_2 and H_2.
- Begin to define the role of promoters in high-alpha catalysts.
- Compare the effectiveness of Ca, Ba and Zn to K as promoters for low-alpha catalysts.

C.0. - Task 3.0. Catalyst Structure and Characterization

The goal of this task is to provide basic analyses (surface area, XRD) of all catalyst prepared and to provide additional techniques as required (Mössbauer, SEM, XPS, etc.) to answer specific questions or to provide basic required characterization data for the catalysts.

Catalyst samples are being extracted to remove the wax for characterization by Sandia and the University of New Mexico.

C.1. Schedule of Activities for Next Quarter

- Complete the wax extraction of selected catalyst samples and ship them to Sandia and the University of New Mexico for characterization.
- Continue to provide the characterization data as required.

D.0. - Task 4.0. Catalyst Testing

The goals of this task are to operate the eight CSTRs, measure catalyst performance, determine the stable phases that exist during synthesis at low and high conversions and to determine the rates of interconversion of iron oxide and carbide.

D.1. Verify the Quality of Data Obtained from the CSTRs.

This task is now completed. The previously unexplained loss and re-establishment of activity has been found to be due to the lowering of the liquid level in the reactor. The conversion data shown in Figure 13 clearly show the loss of activity when rewax (wax from the reactor) was collected on a daily basis in the first 500 hours of the run. When the sampling of the rewax was stopped the activity recovered to approximately the initial level. Repeating this cycle produced a loss and gain of activity again. From these data, it was suggested that removing the reactor wax lowered the liquid level by physically removing the wax material and thus allowed more of the lighter material including the start-up oil to be removed from the reactor. After most of the start-up oil was removed and the reactor contained a sufficient amount of FTS wax, the reactor liquid level became stabilized and sampling of the reactor wax could be done without affecting the activity.

The problem of removing wax with high-alpha catalysts has been solved by employing a 2 micron filter. Figure 14 shows the conversion data for a run which lasted over 1200 hours. As can be seen, there was no difficulty in operations for this run.

The Hewlett-Packard ChemStation was installed in three stages to four gas chromatographs. The third and final installation was completed on March 27, 1995. Two days later a squirrel was caught in our substation and caused a power outage. This power outage knocked our ChemStation data system out. This caused considerable

down-time but the problem has been solved and corrected. We are now beginning to operate all four gas chromatographs on-line to the data system.

D.2. Measure Catalyst Performance

During this quarter the kinetics of the Fischer-Tropsch synthesis was studied over the best low-alpha catalyst developed so far at the CAER to provide optimum reaction conditions for the utilization of this catalyst. Conversion data were obtained over the catalyst for a wide range of conversion levels (15-85%). The partial pressures and reaction rates of the reaction components were calculated from the analysis of the reaction products. A number of possible reaction rate expressions were tested with the experimental data and an optimum reaction rate expression was developed for this catalyst.

Several kinetic studies have been carried out over iron-based catalysts as evidenced in the literature (1,2,3,4). The studies have been over fused iron catalysts as well as precipitated iron catalysts. Table 4.1.A.1 lists the reaction rate expressions proposed. From the nature of the reaction rate expressions developed, it can be clearly seen that a consensus is lacking in the literature. Especially important is the role played by water and/or carbon dioxide in the suppression of the reaction rate at higher synthesis gas conversions.

The Fischer-Tropsch reaction was carried out in a 1-liter stirred tank slurry reactor. A schematic of the reaction system is given in Figure 4.1.A.1. The catalyst used is a precipitated iron catalyst (62 wt.% Fe) containing 4.4 atomic percent Silicon and 0.5 wt.% potassium. The iron catalyst containing silicon (5.09 g) was placed in the reactor with 290 g of C_{28} paraffin and 0.0159 g of potassium was added in the form of potassium tertiary-

butoxide. The reactor pressure was built up to 175 psig under CO atmosphere and subsequently heated to 270°C at a rate of 2°C/min. Pretreatment of the catalyst was carried out at 270°C, 175 psig using CO at a flow rate of 13.345 NL/hr for 24 hours. Subsequently synthesis gas flow was started at a H_2/CO ratio of 0.67. About two days were required before the catalyst reached steady state as evidenced by the constant conversion of synthesis gas. Subsequently, the space velocity of the synthesis gas was varied between 5 and 70 and conversions of CO, H_2, and the formation of various products were measured with a period of approximately 24 hours at each space velocity. The H_2/CO ratio of the feed synthesis gas was kept constant at 0.67 at all the space velocities. Periodically during the run, the catalyst activity was measured at pre-set "standard" conditions to check for catalyst deactivation.

The vapor stream at the reactor outlet was passed through two condensers maintained at different temperatures of 100 and 0°C. The flow rate of the uncondensed gas as well as its composition was measured by a soap-bubble flow meter and on-line gas chromatographs. The condensed liquids in the condensers were collected during a mass balance period and separated into a hydrocarbon and aqueous phase. The two phases were analyzed separately to obtain the weight/mole fractions of water, oxygenates and hydrocarbons in the collected liquids.

The conversions of CO, H_2 and synthesis gas are calculated from the inlet and outlet flow rates of these components from the reactor

$$X_{CO} = (CO_{in} - CO_{out})/CO_{in} \quad (1a)$$

$$X_{H_2} = (H_{2_{in}} - H_{2_{out}})/H_{2_{in}} \quad (1b)$$

$$C_{CO+H_2} = ((CO_{in} - H_{2_{in}}) - (CO_{out} + H_{2_{out}}))/(CO_{in} + H_{2_{in}}) \quad (1c)$$

Since the reactor used is a continuous-flow stirred tank reactor (CSTR), the reaction rates of disappearance of CO and H_2 and the rates of formation of products are obtained directly from the observed conversions. Further the reaction rates are uniform throughout the reactor as the partial pressures of the reactants and products are uniform throughout the reactor.

The rate of disappearance of CO and H_2 can be calculated from

$$-r_{CO+H_2} = 22.4\ SV\ X_{CO+H_2} \quad (2a)$$

$$-r_{CO} = 22.4\ SV\ X_{CO} \quad (2b)$$

$$-r_{H_2} = 22.4\ SV\ X_{H_2} \quad (2c)$$

where SV is the space velocity of the synthesis gas in terms of normal liters per hour per gram of iron.

The rates of formation of the reaction products, CO_2 and H_2O, are calculated from the output flow rates of the products

$$r_{CO_2} = CO_{2_{out}} / W_{Fe} \quad (3a)$$

$$r_{H_2O} = H_2O_{out} / W_{Fe} \quad (3b)$$

where W_{Fe} is the grams of iron in the reactor. The rate of formation of the hydrocarbons is difficult to measure as a significant amount of the heavier hydrocarbons remain in the reactor liquid.

The partial pressures of the various components in the reactor are calculated from their mole fractions in the reactor outlet stream. Here the condensed product liquid in the condensers must be taken into account. Hence the composition of the product liquids is measured and averaged over the total mass balance period to obtain the moles per hour of the liquid products so as to compare the results with the composition of the uncondensed gas from the on-line gas chromatographs and thus obtain the mole fractions of each product and unconverted reactant in the vapor phase in the reactor.

$$P_{CO} = y_{CO,out} P_{total} \quad (4a)$$

$$P_{H_2} = y_{H_2,out} P_{total} \quad (4b)$$

$$P_{CO_2} = y_{CO_2,out} P_{total} \quad (4c)$$

$$P_{H_2O} = y_{H_2O,out} P_{total} \quad (4d)$$

$$P_{HC} = y_{HC,out} P_{total} \quad (4e)$$

The reaction run lasted for approximately 12 days. The catalyst activity at pre-set standard conditions during this run is shown in Figure 4.1.A.2. As shown in this figure the catalyst activity remained practically constant during the course of the reaction run. Figure

4.1.A.2 also shows that the experimental error in the measurement of percentage conversion is about 2%.

Figure 4.1.A.3 shows the conversions of CO, H_2 and total conversion of CO and H_2 with space time in the reactor. The change in the percent conversion is much faster at low space times than it is at higher space times. Further at low space times the conversion of H_2 is greater than the conversion of CO while at higher space times the situation is reversed. The total CO and H_2 conversion at which the conversions of both CO and H_2 become equal is about 67%.

Figure 4.1.A.4 shows the calculated partial pressures of the various components in the vapor phase in the reactor as a function of space time. As expected, the partial pressures of CO and H_2 decrease with space time while the partial pressures of CO_2 and hydrocarbons increase with space time. The partial pressure of water initially increases with space time and then decreases indicating that it is an intermediate. This is also as expected since the water gas shift reaction consumes water formed from the Fischer-Tropsch synthesis.

Figure 4.1.A.5 shows the calculated rates of disappearance of CO, H_2, synthesis gas and the rates of formation of water and CO_2 with space time. The rate of disappearance of H_2 decreases with space time as does the rate of formation of water. The rate of disappearance of synthesis gas is approximately constant at small space times and then decreases monotonically with increasing space time. Both the rate of disappearance of CO and the rate of formation of CO_2 pass through a maximum with increasing space time.

Figure 4.1.A.6 shows the hydrocarbon selectivities obtained at the different space velocities used in this study. The probability of chain growth, α, is practically the same at all the space velocities studied and has a value of 0.74 over this particular catalyst.

The implications of the data obtained in this kinetic study are discussed in this section. It is of interest to note the relative conversions of CO and H_2 as the space time in the reactor is increased. The conversion of H_2 is greater than the conversion of CO at low space times while the reverse is true at higher space times. At a total synthesis gas conversion of between 65-70%, the H_2/CO ratio of the product gas is equal to the H_2/CO ratio of the incoming synthesis gas. This implies that at higher conversions, H_2 is being formed faster by the water gas shift reaction than it is being depleted by the formation of hydrocarbons.

The partial pressure of water over this catalyst is approximately constant over the entire range of synthesis gas conversions studied. Further, its partial pressure is smaller than the partial pressures of the other reaction components especially at high conversion levels. This implies that the catalyst used is a good water gas shift catalyst and converts the greater amounts of water formed by the Fisher-Tropsch reaction at high synthesis gas conversions.

The reaction rates of formation of products and disappearance of reactants are used to calculate the rate of the Fischer-Tropsch reaction and the rate of the water gas shift reaction from:

$$-r_{WGS} = R_{CO_2} \quad (5a)$$

$$-r_{FT} = (-r_{CO}) - r_{CO_2} \quad (5b)$$

These rates are plotted as a function of total synthesis gas conversion in Figure 4.1.A.7. As shown in this figure, the rate of the Fischer-Tropsch reaction is always greater than the rate of the water gas shift reaction. However, at high conversions of synthesis gas (above 55%) the rate of the water gas shift reaction closely approaches the rate of the Fischer-Tropsch reaction. Up to about 55% conversion the rate of the Fischer-Tropsch reaction is approximately constant after which it monotonically decreases. In contrast, the rate of the water gas shift reaction passes through a maximum with increasing synthesis gas conversion.

Carbon monoxide can get converted to either hydrocarbons (Fischer-Tropsch) or carbon dioxide (water gas shift). Since hydrocarbons are the more desirable products, it is of interest to see how the fraction of CO converted to hydrocarbons varies with the total synthesis gas conversion. This is plotted in Figure 4.1.A.8 and shows that the fraction of CO converted producing hydrocarbons decreases as the total synthesis gas conversion increases. This implies that at higher synthesis gas conversions a larger amount of CO is being converted to the undesirable product CO_2 and not to hydrocarbons.

An important conclusion to be drawn from this is that it would be more desirable to carry out the Fischer-Tropsch synthesis at intermediate conversions and have either two reactors in series or operate a single reactor with recycle. At intermediate conversions the fraction of CO being converted to the undesirable product CO_2 is lower. Further, the

exit gas from the reactor has about the same H_2/CO ratio as that of the inlet gas to the reactor so that the second reactor or the recycle stream would have the same H_2/CO ratio as the first reactor.

The experimental data obtained in this study also allow us to test the various reaction rate expressions proposed in the literature for Fischer-Tropsch synthesis over iron-based catalysts. For the purpose of testing these rate expressions against the experimental data they are rearranged so as to obtain a linear relationship. The experimental data are then plotted according to this linear relationship to determine if a straight line gives a good fit to the data obtained. The rearranged reaction rate expressions from those given in Table 4.1.A.1 are given below:

$$P_{H_2}/-r_{CO+H_2} = (1/k) = (b/k)\ (P_{H_2O}/P_{CO}) \qquad \textbf{(6a)}$$

$$P_{H_2}/-r_{CO+H_2} = (1/k) = (b/k)\ (P_{H_2O}/P_{CO}P_{H_2}) \qquad \textbf{(6b)}$$

$$P_{H_2}/-r_{CO+H_2} = (1/k) = (b/k)\ (P_{CO_2}/P_{CO}) \qquad \textbf{(6c)}$$

Figures 4.1.A.9, 4.1.A.10 and 4.1.A.11 show the experimental data plotted according to these linear relationships. As shown in these figures, none of the proposed rate expressions in the literature are able to give a good fit to the data obtained in this study. However, a reaction rate expression which represents the experimental data well is given below:

$$-r_{CO+H_2} = k\ P_{CO}\ P_{H_2}/(1 + K_{CO}P_{CO}) \qquad \textbf{(7a)}$$

Rearranging this expression, we get:

$$P_{CO}\ P_{H_2} / -r_{CO+H_2} = (1/k) + (K_{CO}/k)\ P_{CO} \qquad (7b)$$

Figure 4.1.A.12 shows the fit of the experimental data to the rearranged rate expression. A reasonably good fit is obtained. This rate expression differs from the proposed rate expressions in the literature in that there is no inhibition of the rate by the reaction products (water and/or CO_2) and no competition between the adsorption of CO and the reaction products (water and/or CO_2). A possible reason for this difference in the case of one of the reaction products, water, is the low and almost constant partial pressures of water obtained over this catalyst at all the space velocities studied. Hence any effect of water on the reaction rate would appear to be low since its partial pressure does not vary much. However, this explanation does not hold for the other reaction product, namely carbon dioxide. In this case, the partial pressure of CO_2 varies considerably with space velocity. Hence it can be concluded that CO_2 does not influence the reaction rate over the catalyst used in this study.

The Fischer-Tropsch synthesis has been studied over the best low-alpha catalyst developed at the CAER. A wide range of synthesis gas conversions were obtained by varying the space velocity. The experimental results show that: (i) the rate of the water gas shift reaction is lower than the rate of the Fischer-Tropsch reaction at low conversions (< 60%) whereas it closely approaches the rate of the Fischer-Tropsch synthesis at high conversions, (ii) the fraction of CO converted to hydrocarbons is higher at low and intermediate conversions whereas it is smaller at high conversions, (iii) the H_2/CO ratio of the product gas is equal to the H_2/CO ratio of the inlet synthesis gas at an intermediate conversion level of 67%. These findings suggest that it would be beneficial to carry out the reaction at intermediate conversions. This would result in an optimum use of CO to

produce hydrocarbons rather than CO_2. High overall conversions can be obtained by either using a second reactor or recycling the product gas using a single reactor. If the intermediate conversion in a single pass is maintained at 67% there would be no need to adjust the H_2/CO ratio of the recycle stream or the feed to the second reactor as the product gas from a single pass would have the same H_2/CO ratio as the feed synthesis gas.

The optimum reaction rate expression for synthesis gas conversion has been developed for this catalyst:

$$-r_{CO+H_2} = k\, P_{CO}\, P_{H_2} / (1 + K_{CO} P_{CO})$$

The rate expression shows that CO is strongly adsorbed on the catalyst and that the reaction products such as water and CO_2 do not inhibit the reaction rate.

Table 4.1.A.1.

Proposed Reaction Rate Expressions Proposed in the Literature over Iron-Based Catalysts

Reference	Reaction Rate Expression
1. Anderson, R.B. in "Catalysis" Vol. IV, Emmett, P.H., Ed., Rheinhold, New York (1956). 2. Atwood, H.E. and C.O. Bennett, I&EC Proc. Des. Dev., 18, 163 (1979).	$-r_{CO+H_2} = K P_{CO} P_{H_2} / (P_{CO} + b P_{H_2O})$
3. Huff, G.A. and C.N. Satterfield, I&EC Proc. Des. Dev., 23, 696 (1984).	$-r_{CO+H_2} = K P_{CO} P_{H_2} / (P_{CO} P_{H_2} + b P_{H_2O})$
4. Ledakowicz, S., H. Nettlehoff, R. Kokuun and W-D. Deckwer, 24, 1043 (1985).	$-r_{CO+H_2} = K P_{CO} P_{H_2} / (P_{CO} + b P_{CO_2})$

D.3. Determine Stable Phases that Exist During Synthesis at High and Low CO Conversion Levels

No scheduled or additional activity to report.

D.4. Obtain Data on Rates Involved in the Interconversion of Iron Oxide and Carbide

No scheduled or additional activity to report.

D.5. Schedule of Activities for Next Quarter

- Continue kinetic work to define role of H_2O and CO_2 at low CO conversion levels.

5. Publications, Presentations and Other Activities

1. Mössbauer study of iron-carbide growth and Fischer-Tropsch activity, Preprints ACS Fuel Chem. Div., 40, 153 (1995) (with K. R. P. M. Rao, F. E. Huggins, G. P. Huffman, R. J. O'Brien and R. J. Gormley).

2. Role of CO_2 in the initiation of chain growth during the Fischer-Tropsch synthesis, Preprints ACS Fuel Chem. Div., 40, 153 (1995) (with L. Xu, S. Bao, L.-M. Tau, B. Chawla and H. Dabbagh).

Figure1. A comparison of the hardness of a Fe_2O_3/SiO_2 catalyst to other materials.

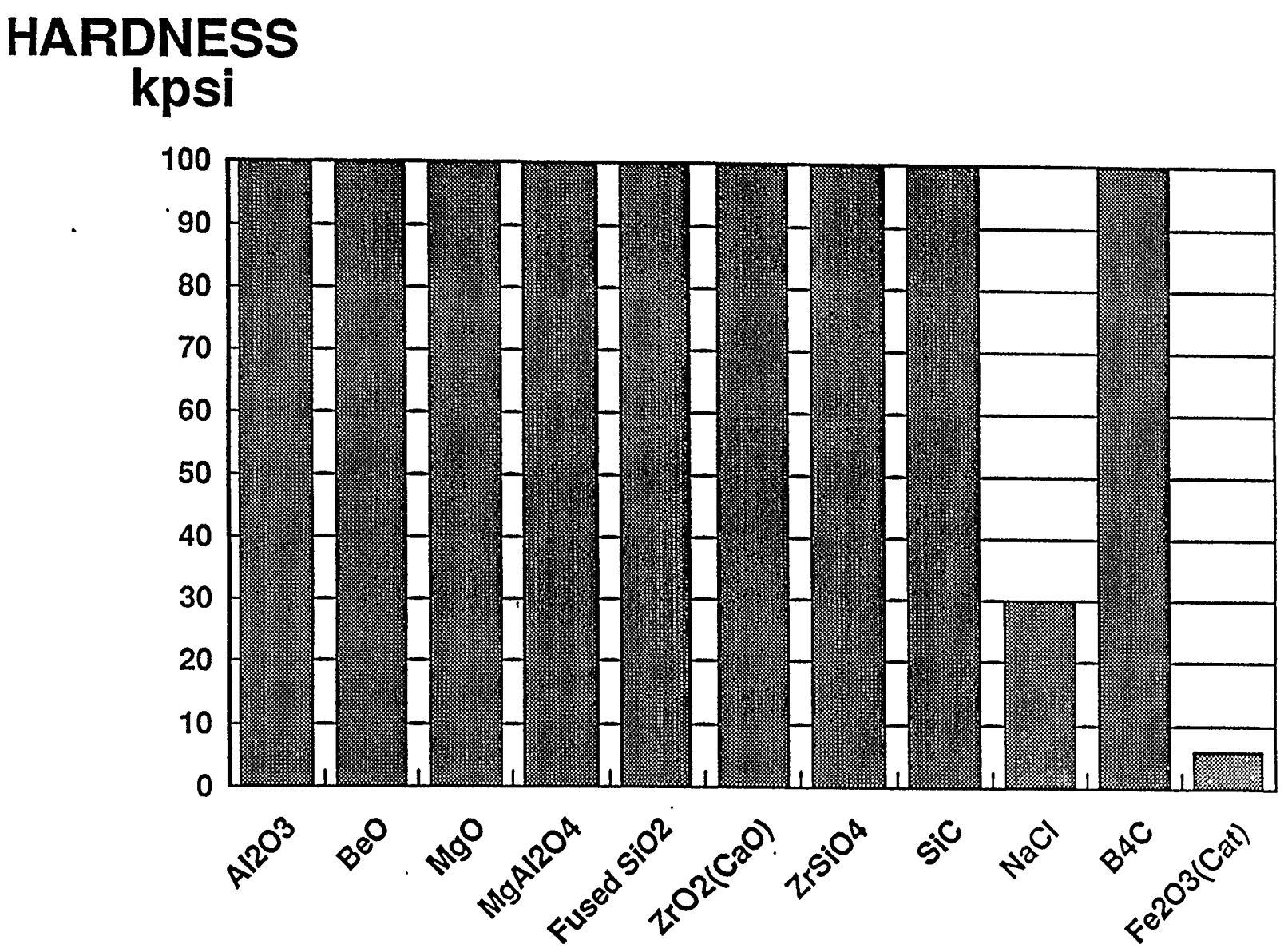

Figure 2. Affect of Cu promotion on synthesis gas activation. O- 100Fe/3.6Si/2.6Cu/0.71K and □- 100Fe/3.6Si/0.71K. Activation and synthesis conditions: 270°C, 13 atm, $H_2/CO=0.7$, s.v.=3.1 NL h^{-1} g^{-1}(Fe).

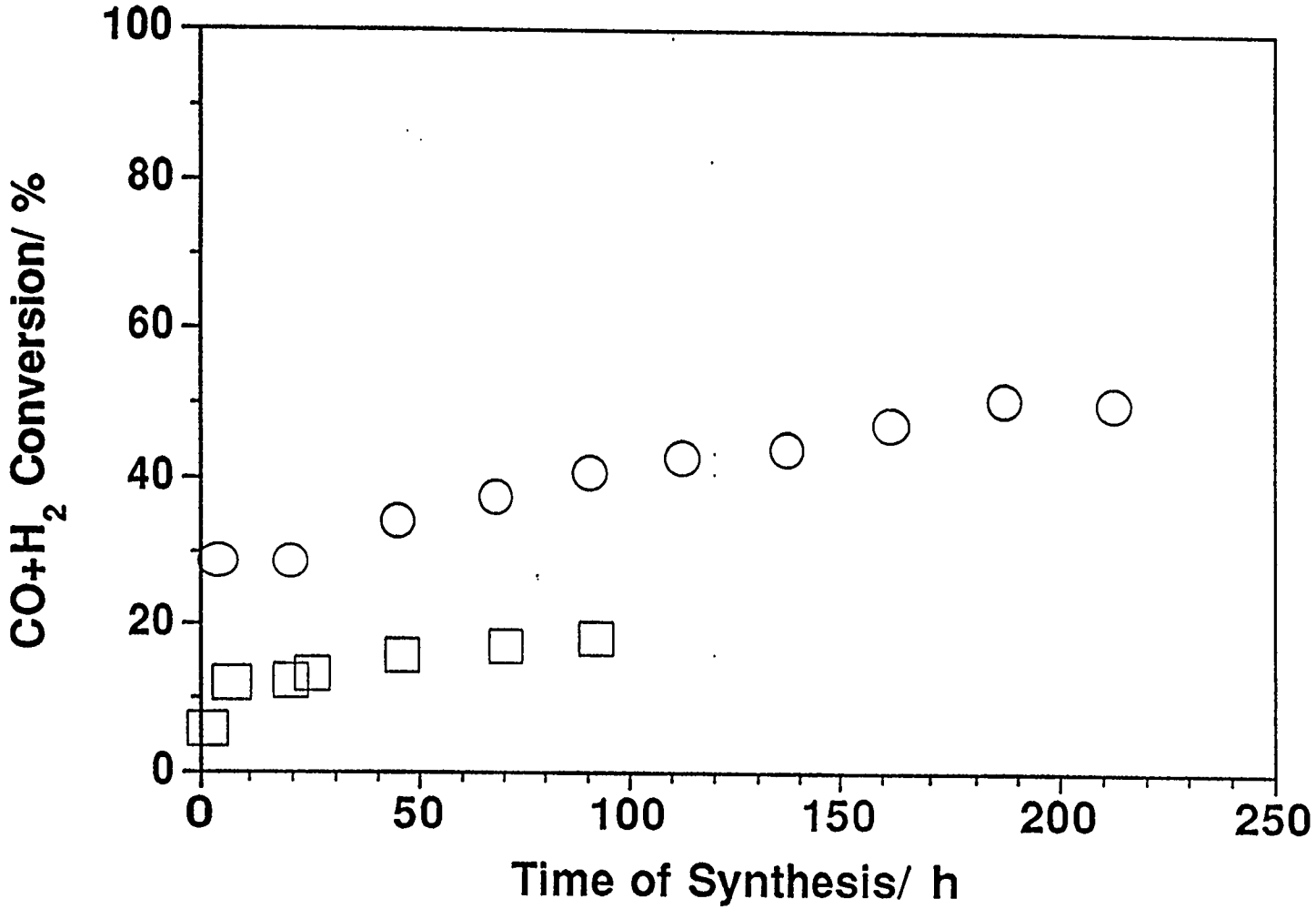

Figure 3. X-ray diffraction results for the 100Fe/3.6Si/2.6Cu/0.71K and 100Fe/3.6Si/0.71K catalysts activated with syngas, $H_2/CO=0.7$, s.v.=3.1 NL h^{-1} g^{-1}(Fe).

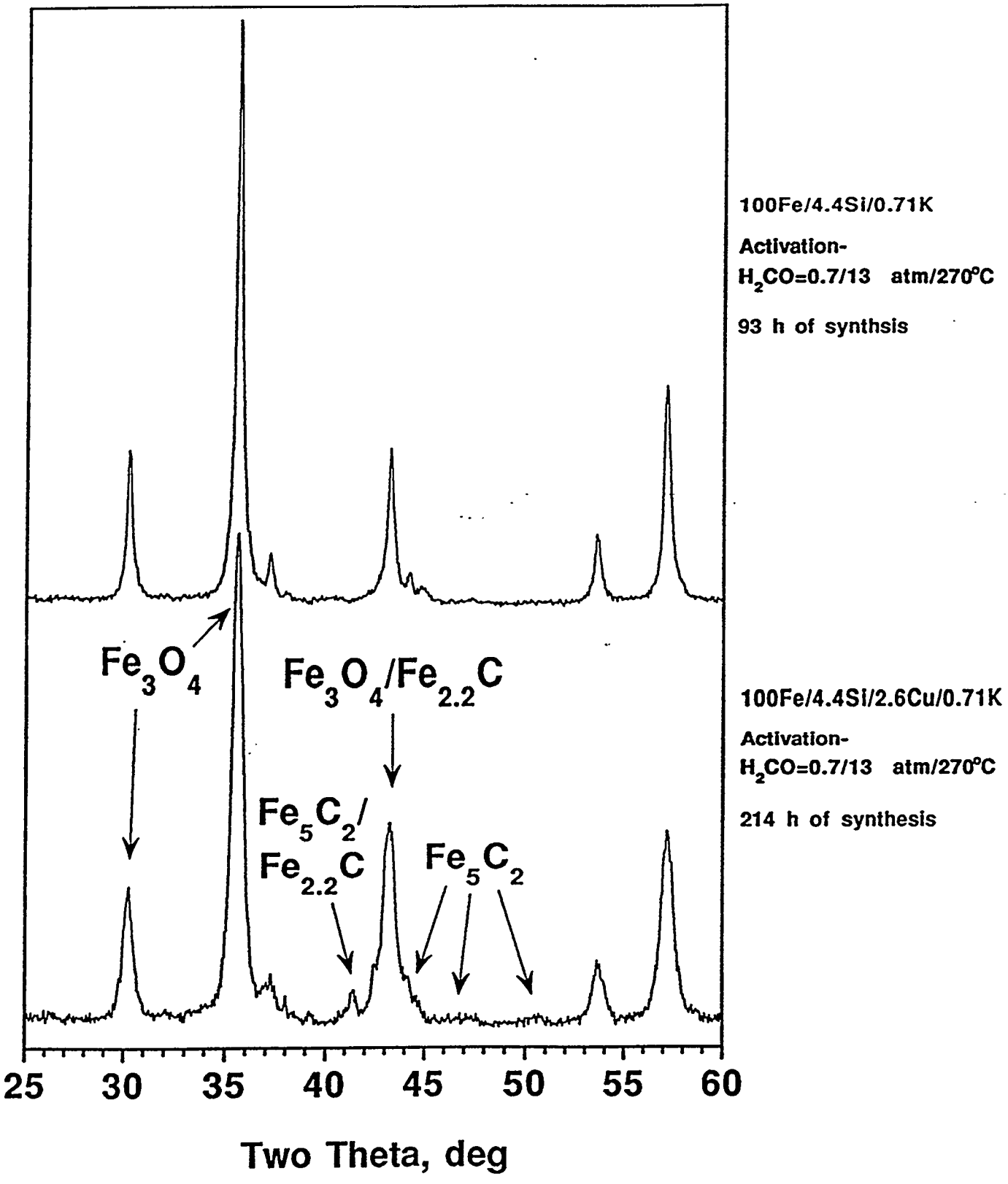

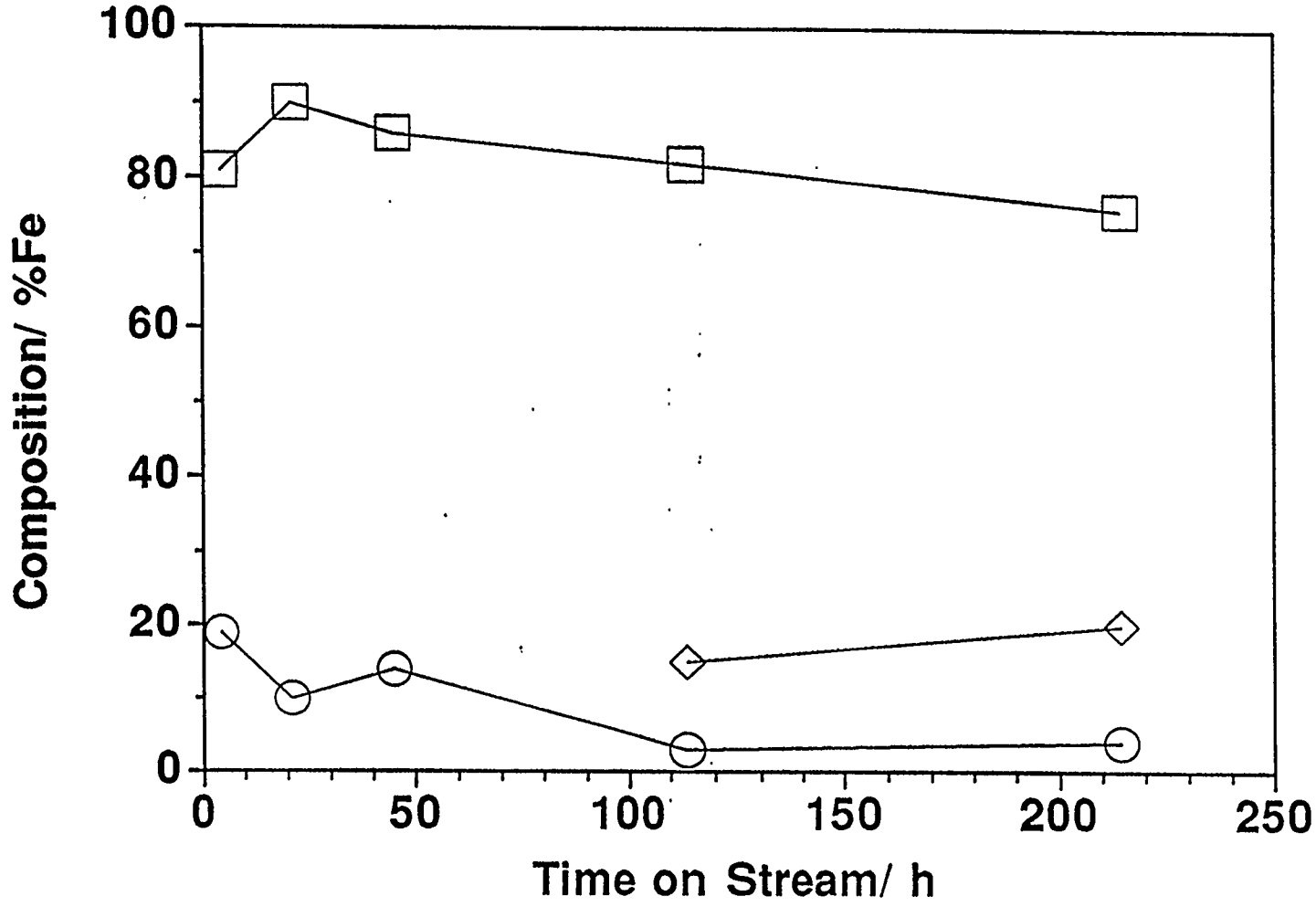

Figure 4. Mössbauer spectroscopy results for the 100Fe/3.6Si/2.6Cu/0.71K catalyst activated at 270°C, 13 atm, $H_2/CO=0.7$. ○- superparamagnetic phase, □- Fe_3O_4, ◇- ε'-$Fe_{2.2}C$. Synthesis conditions: $H_2/CO=0.7$ at 13 atm and 270°C.

Figure 5. CO conversion vs. time on stream for the 100Fe/3.6Si/0.71K catalyst activated with $H_2/CO=0.7$ at 13 atm and O- 270 °C and □- 300 °C. Synthesis conditions: $H_2/CO=0.7$ at 13 atm and 270 °C.

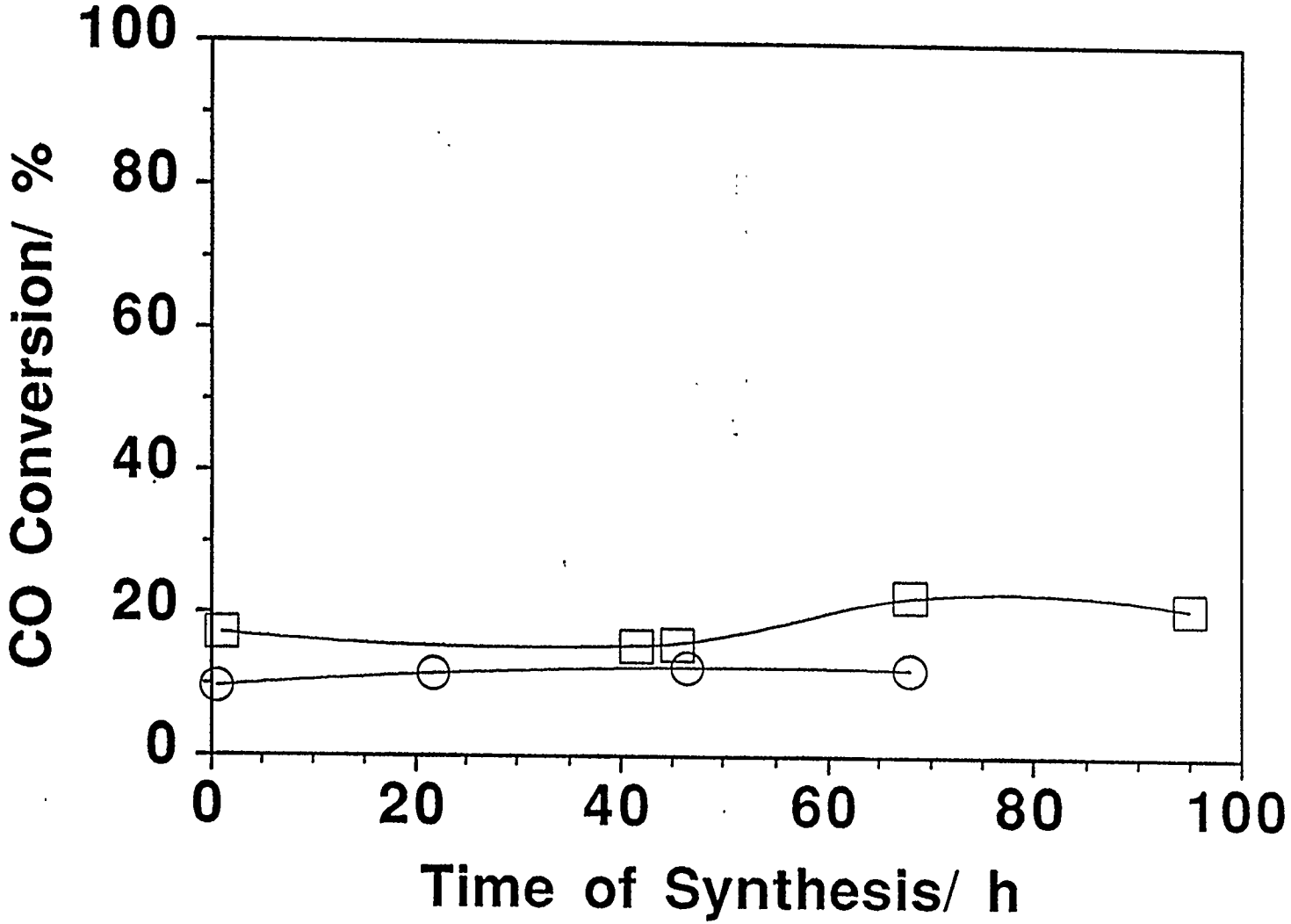

Figure6. CO conversion vs. time on stream for the 100Fe/3.6Si/0.71K catalyst activated at 270°C and 13 atm with ○- CO, ◇- $H_2/CO=0.1$ and □- $H_2/CO=0.7$. Synthesis conditions: $H_2/CO=0.7$ at 13 atm and 270°C.

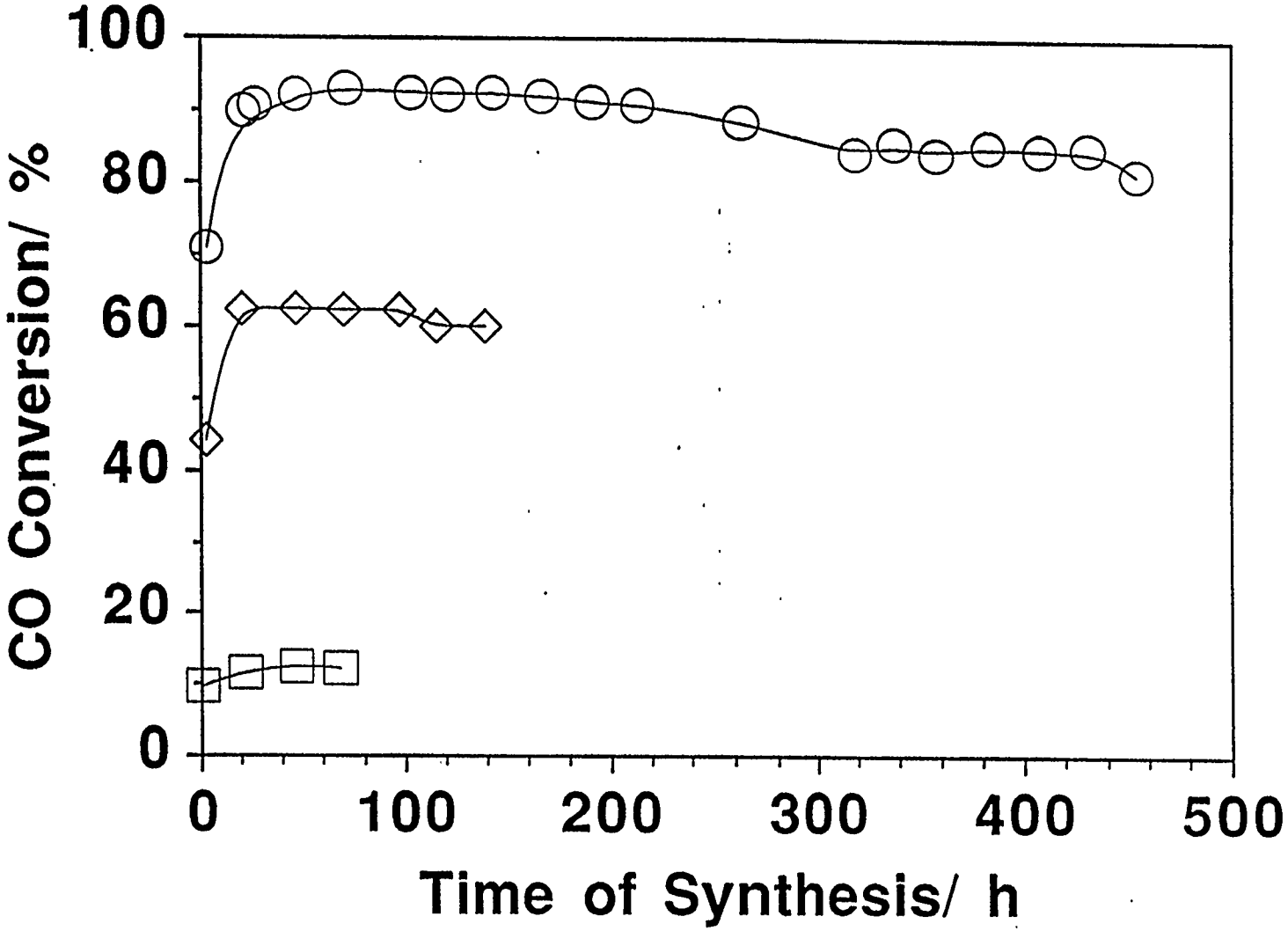

Figure7. Comparison of CO conversion vs. time on stream for the 100Fe/3.6Si/0.71K catalyst activated with $H_2/CO=0.7$, 270°C at ⊙- 13 atm and □- 1 atm. Synthesis conditions: $H_2/CO=0.7$ at 13 atm and 270°C.

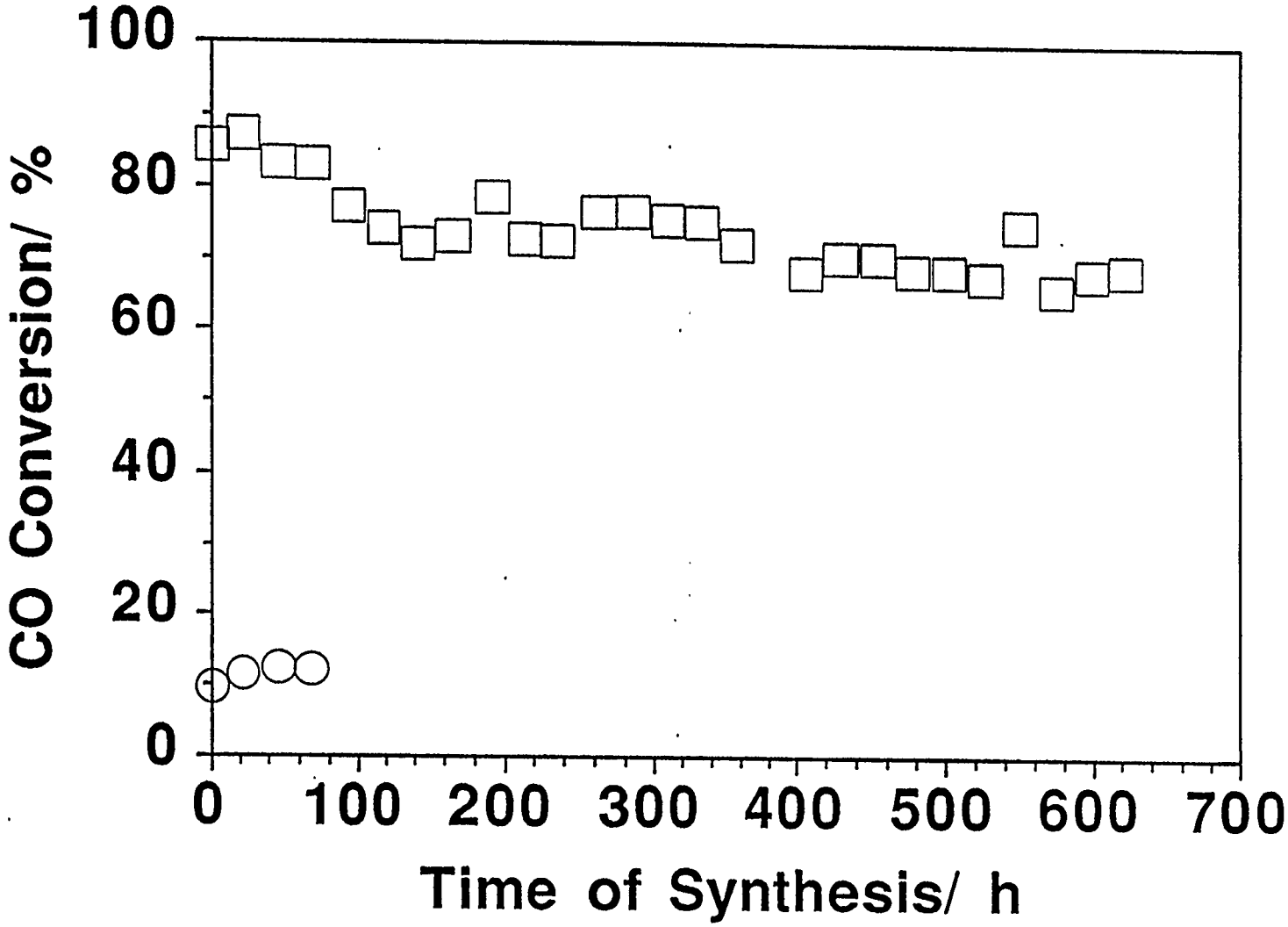

Figure 8. Comparison of CO conversion vs. time on stream for the 100Fe/4.4Si/1.0K catalyst activated at 270°C and 1 atm with ○- CO and □- H_2/CO=0.7. Synthesis conditions: H_2/CO=0.7 at 13 atm and 270°C.

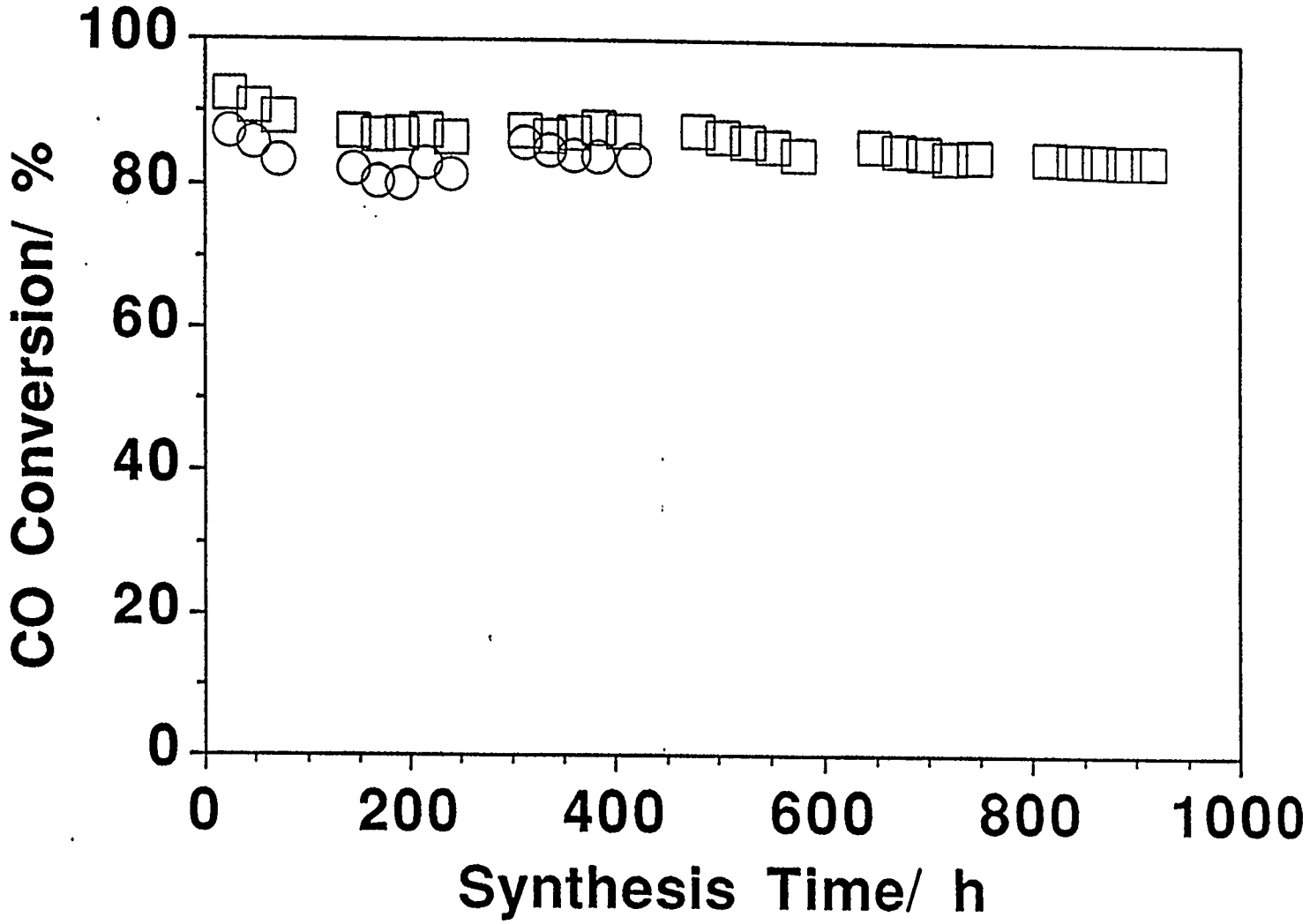

Figure 9. Comparison of CO conversion vs. time on stream for the 100Fe/4.4Si/1.0K catalyst activated with CO for 24 h at C 270 °C and ○- 13 atm and □- 1 atm. Synthesis conditions: $H_2/CO=0.7$ at 13 atm and 270 °C.

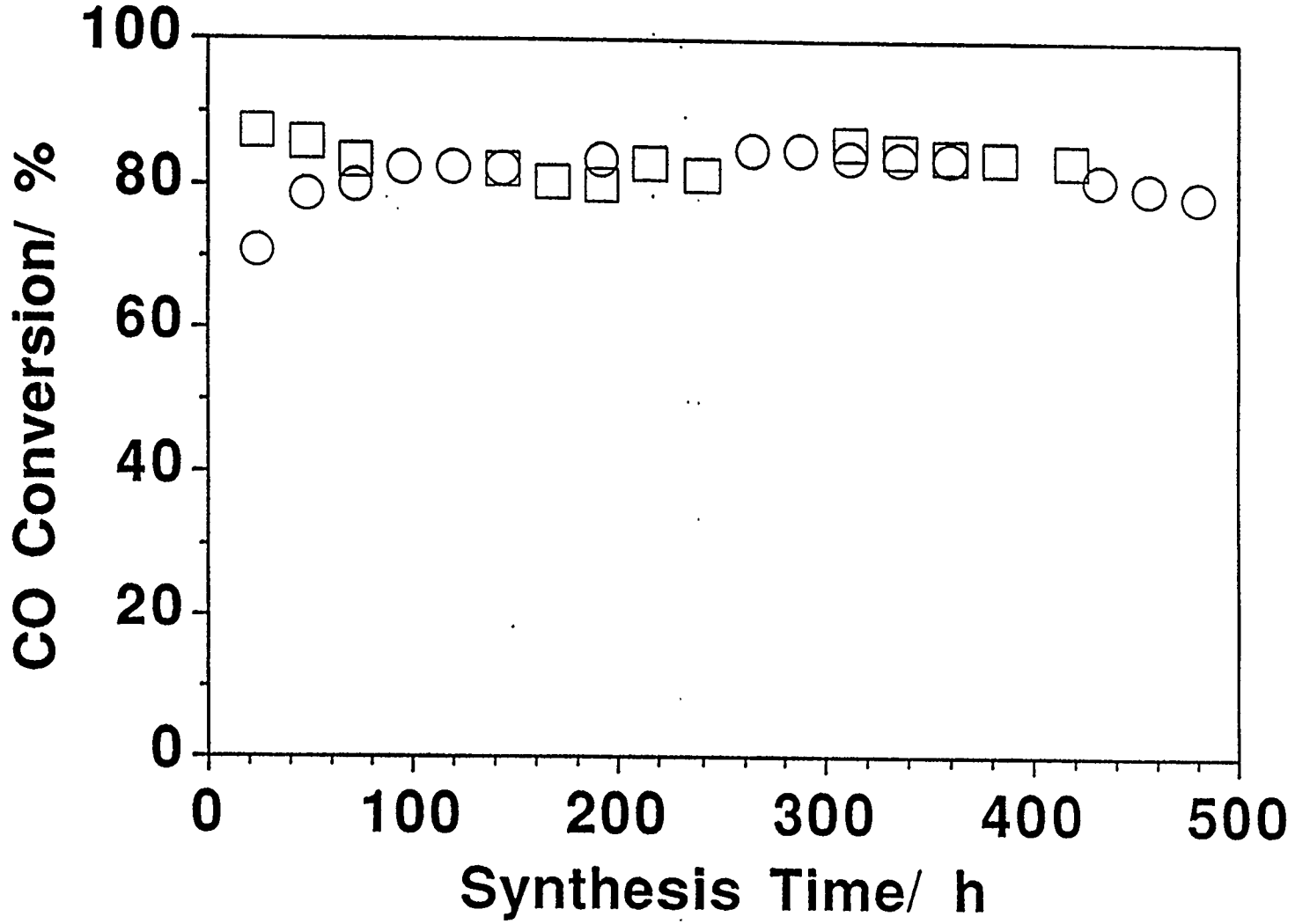

Figure 10. Comparison of X-ray diffraction results for the 100Fe/3.6Si/0.71K catalyst activated with $H_2/CO=0.7$ or CO at 13 atm or 1 atm.

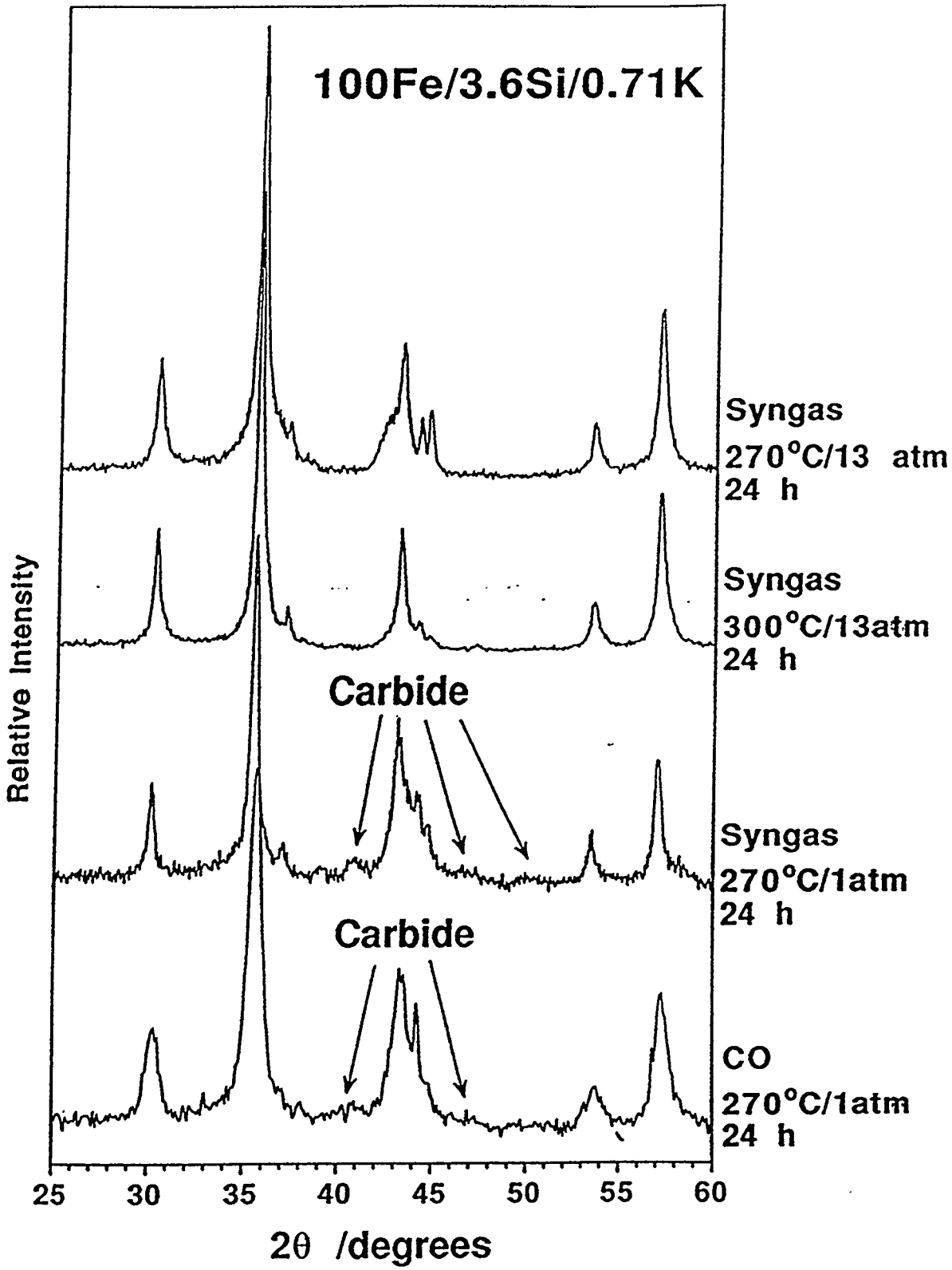

Figure 11. Comparison of the CO conversion vs. time on stream for the 100Fe/3.6Si/0.71K catalyst. □- activated with CO at 270°C, 13 atm for 24 h and ○- activated with $H_2/CO=0.7$ at 270°C and 13 atm followed by a 22 h treatment with CO at 270°C and 13 atm. Synthesis conditions: $H_2/CO=0.7$ at 13 atm and 270°C.

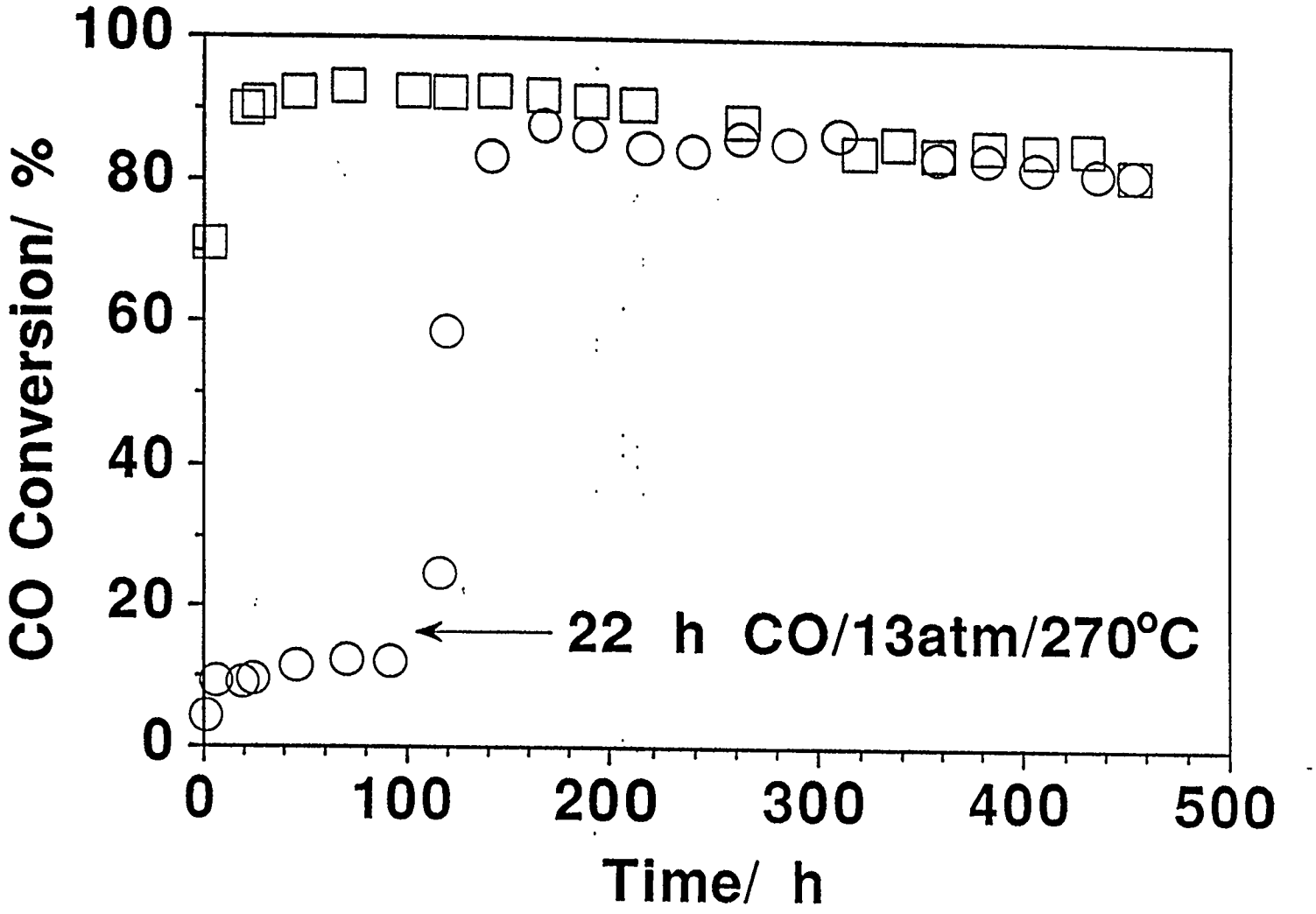

Figure 12. Mössbauer spectroscopy results for the 100Fe/3.6Si/0.71K catalyst activated with $H_2/CO=0.7$ at 270 °C and 13 atm followed by a 22 h treatment with CO at 270 °C and 13 atm. Synthesis conditions: $H_2/CO=0.7$ at 13 atm and 270 °C. ○- superparamagnetic phase, □- Fe_3O_4 and ◇- iron carbide.

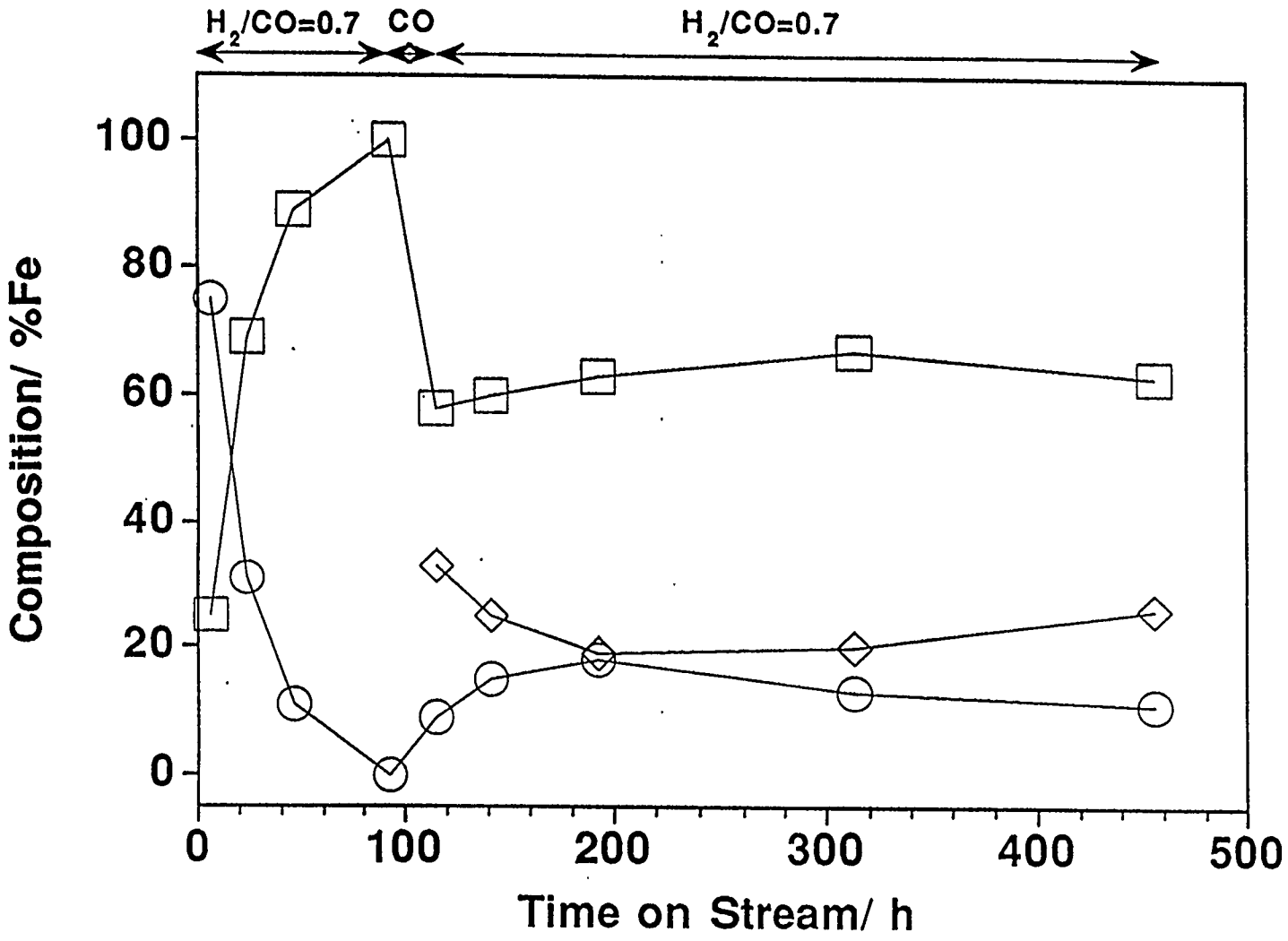

Fig 13. **RLS4.4 Si/150 Cyclone (LGX170 R1)**

Cat. treated at 300 oC, 1 atm. in CO+H2

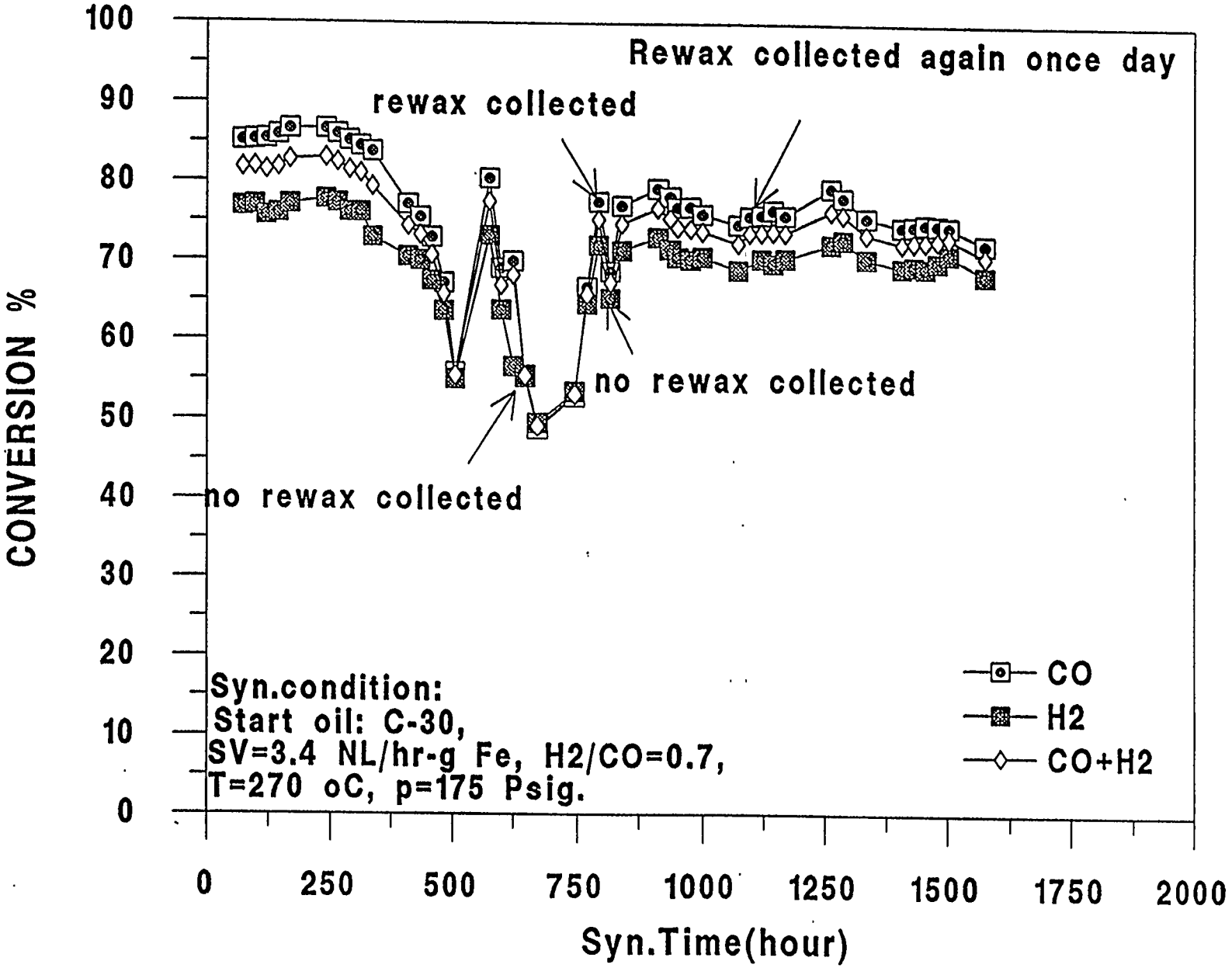

Fig 14. RLS4.4 Si/150 Cyclone (LGX171 R3)

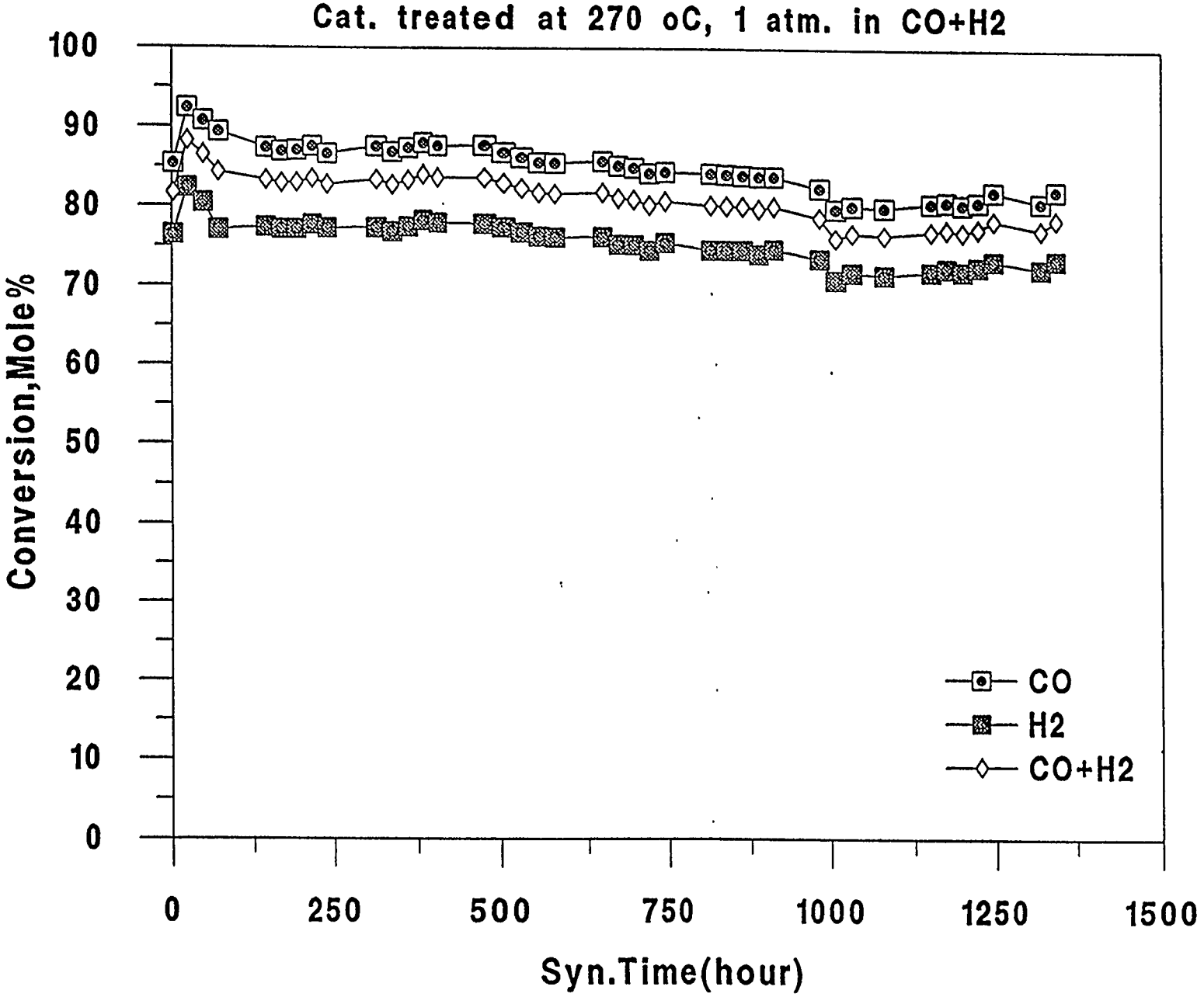

Figure 4.1.A.1 Fischer-Tropsch CSTR Reactor

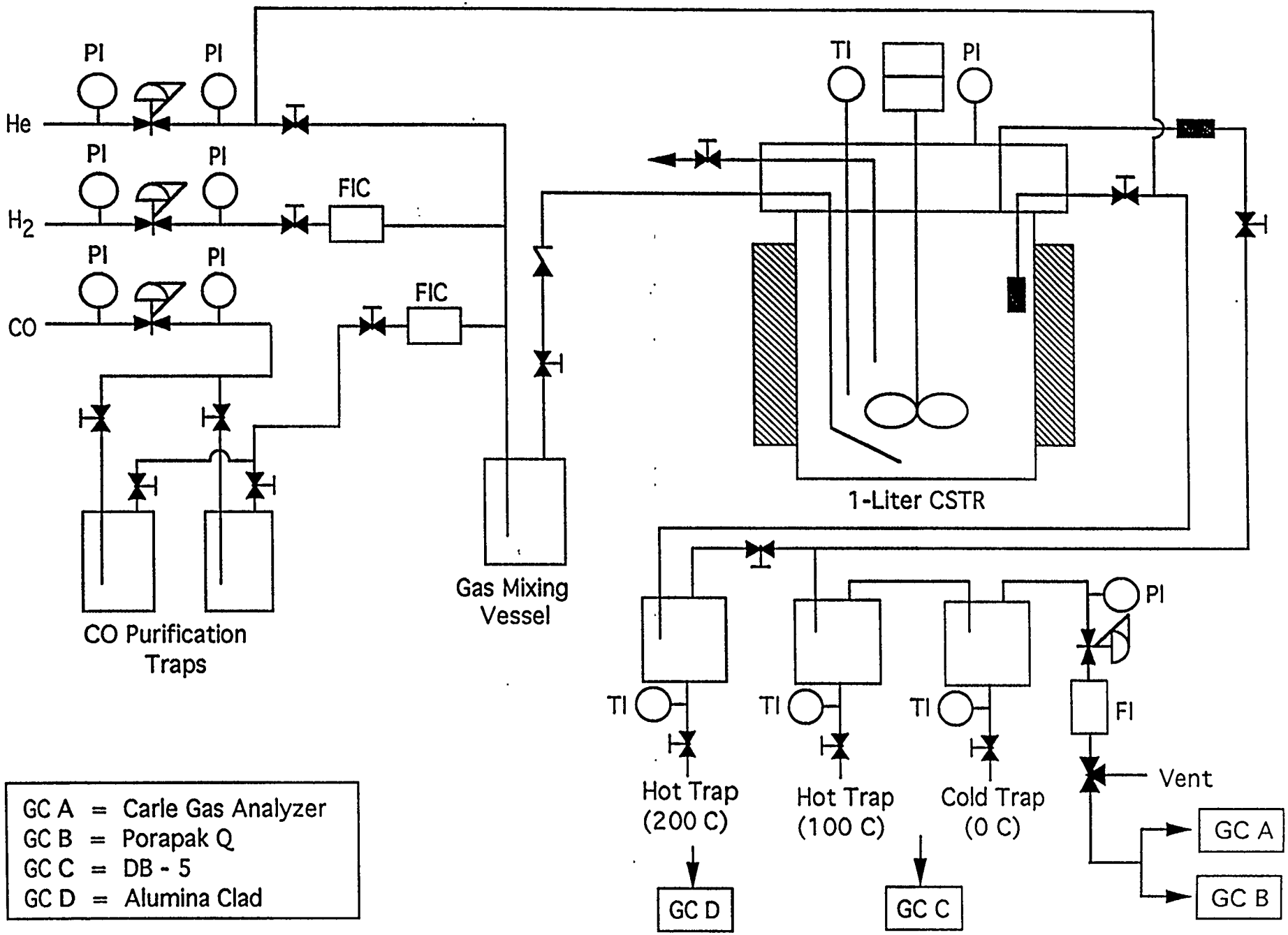

Figure 4.1.A.2 Conversion of Synthesis Gas at "Pre-set" Standard Conditions

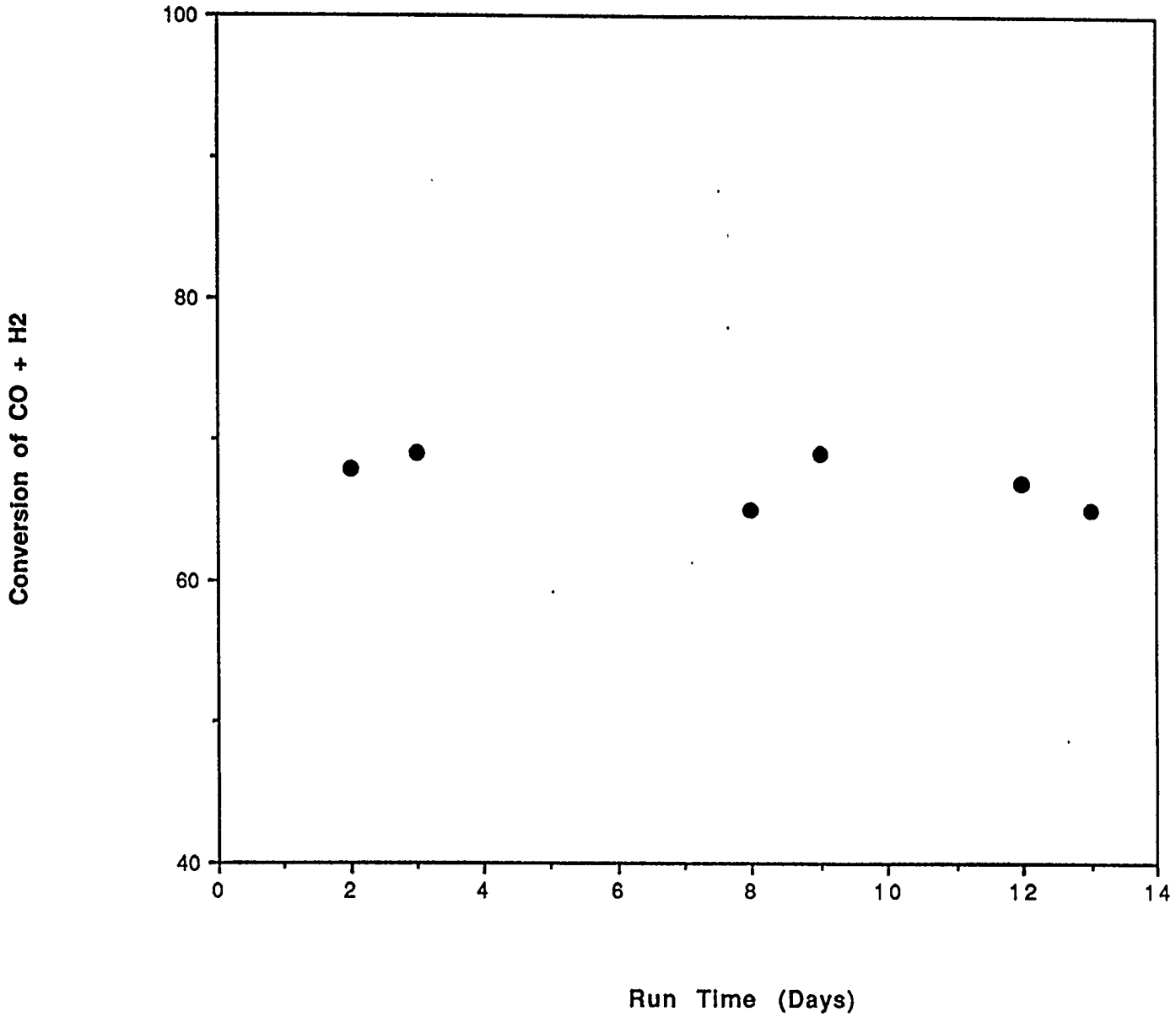

Figure 4.1.A.3 Conversions of Reactants versus Space Time

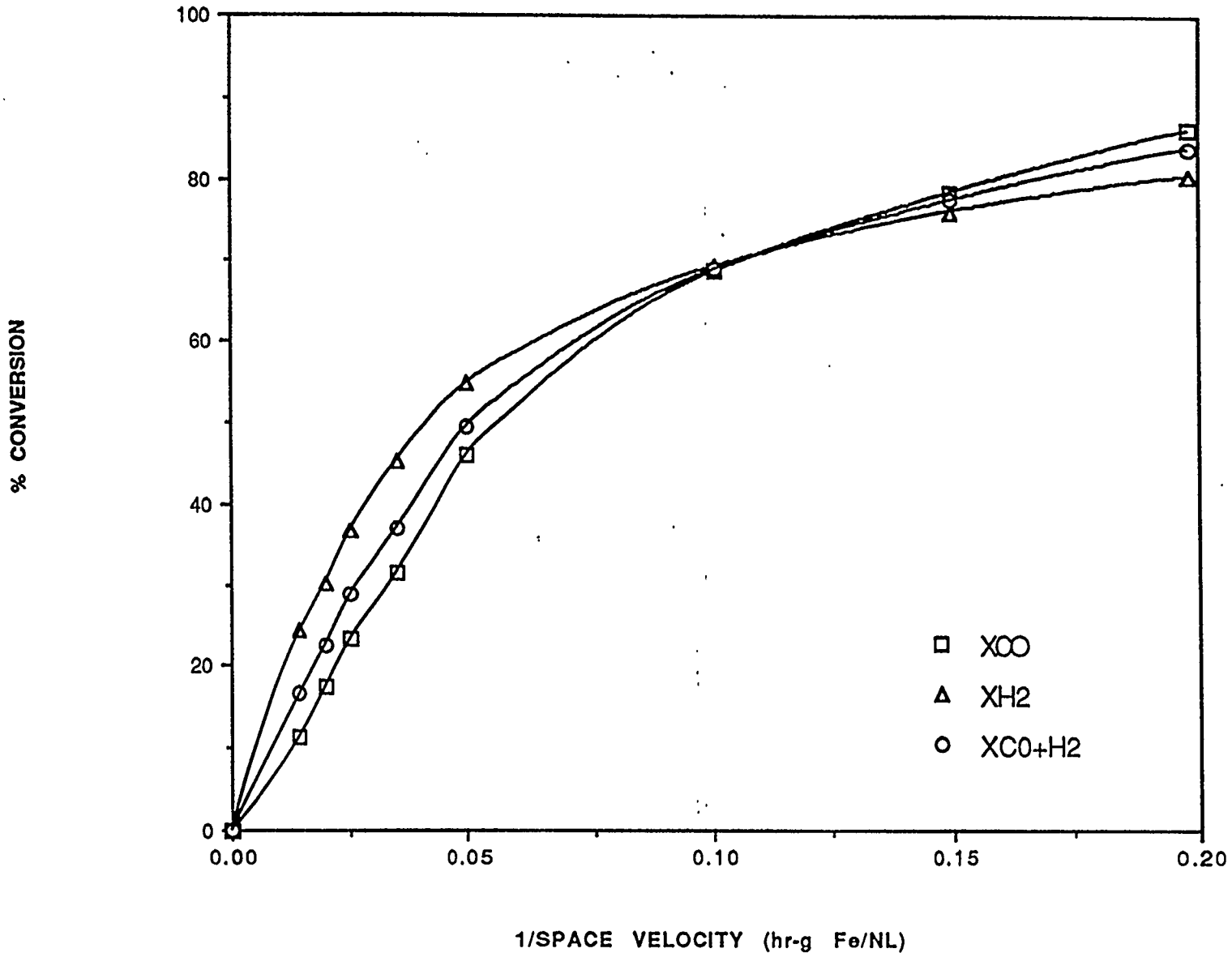

Figure 4.1.A.4 Partial Pressures of Reaction Components

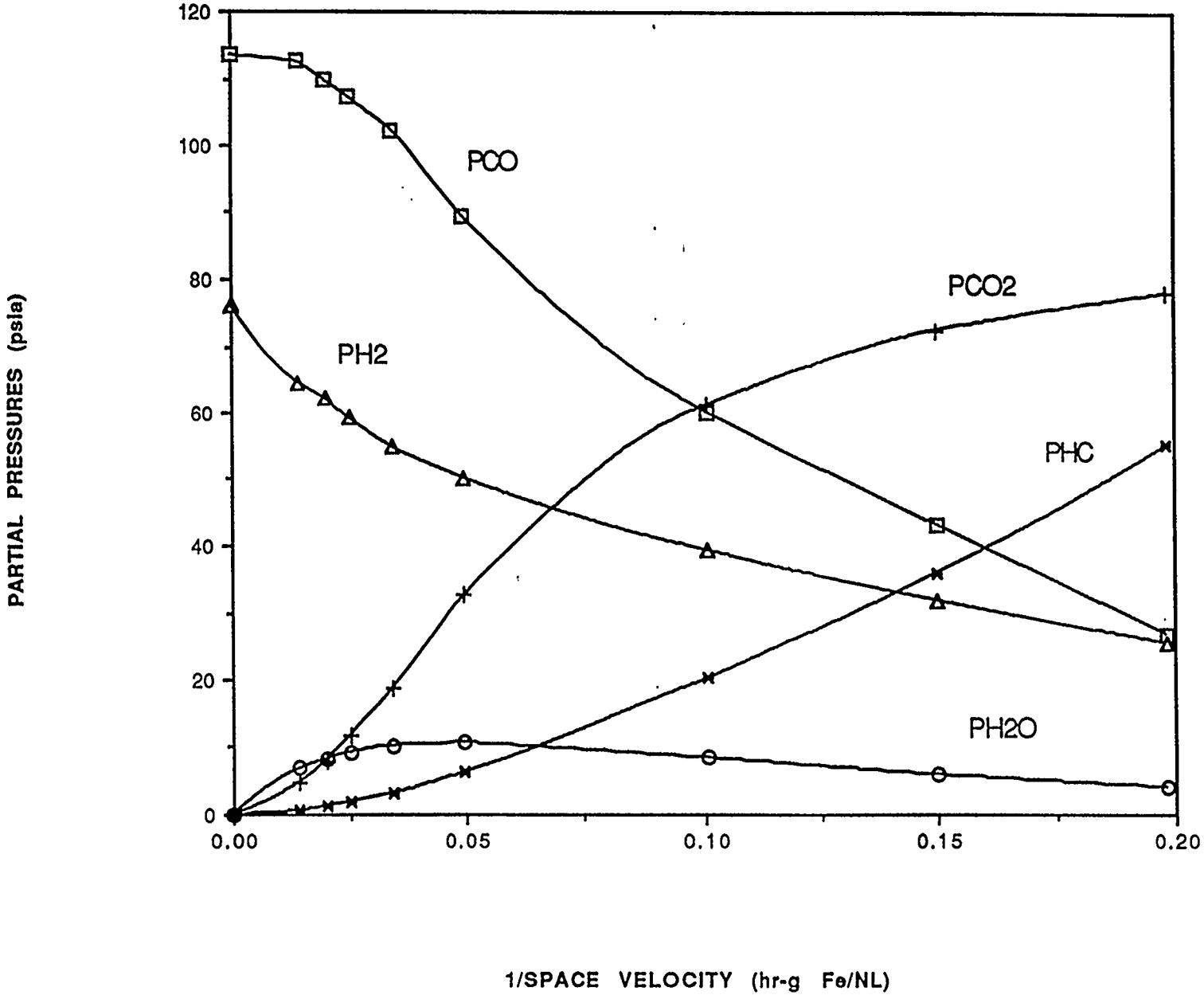

Figure 4.1.A.5 Rates of Disappearance or Formation

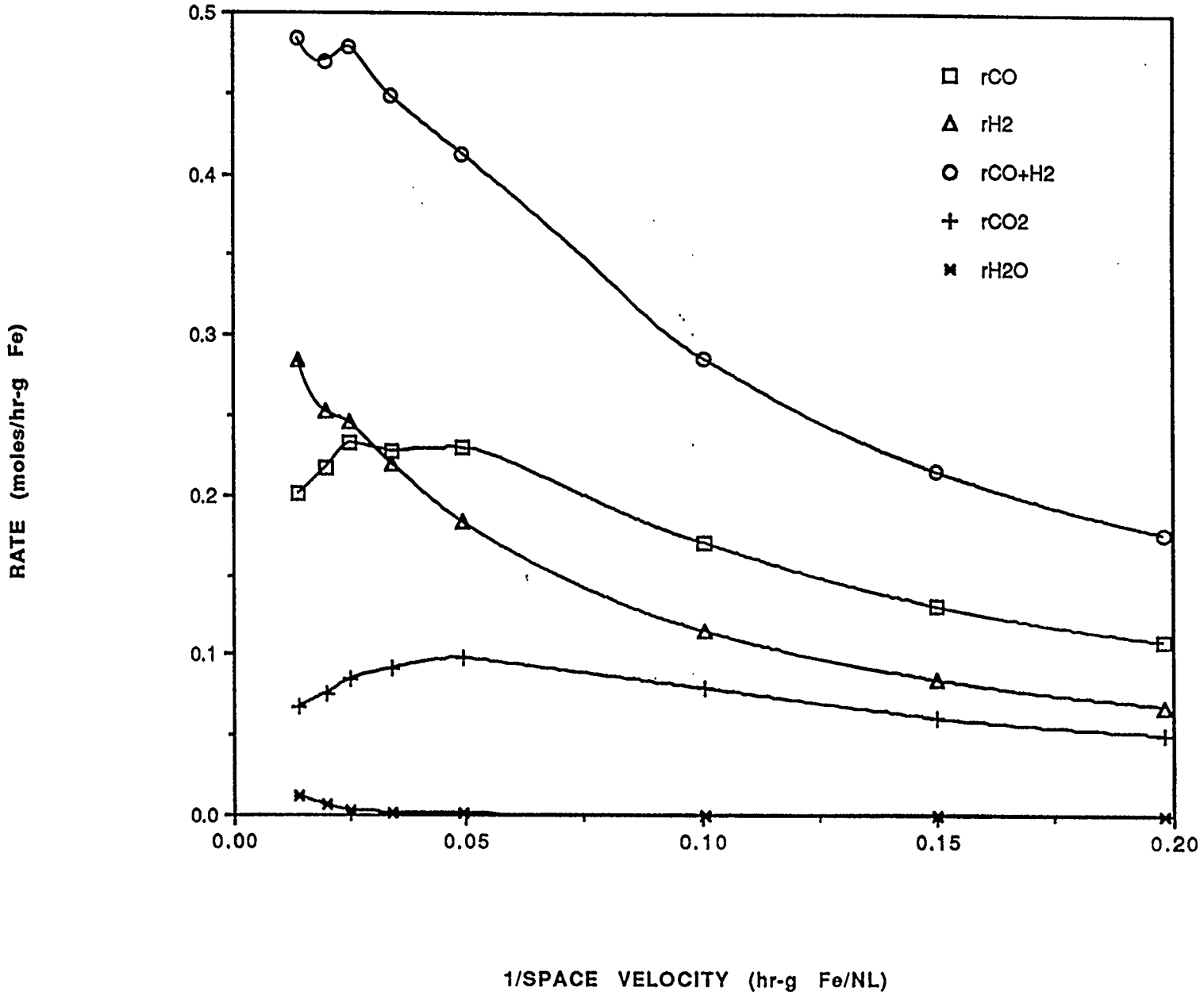

Figure 4.1.A.6 Hydrocarbon selectivities at different space velocities

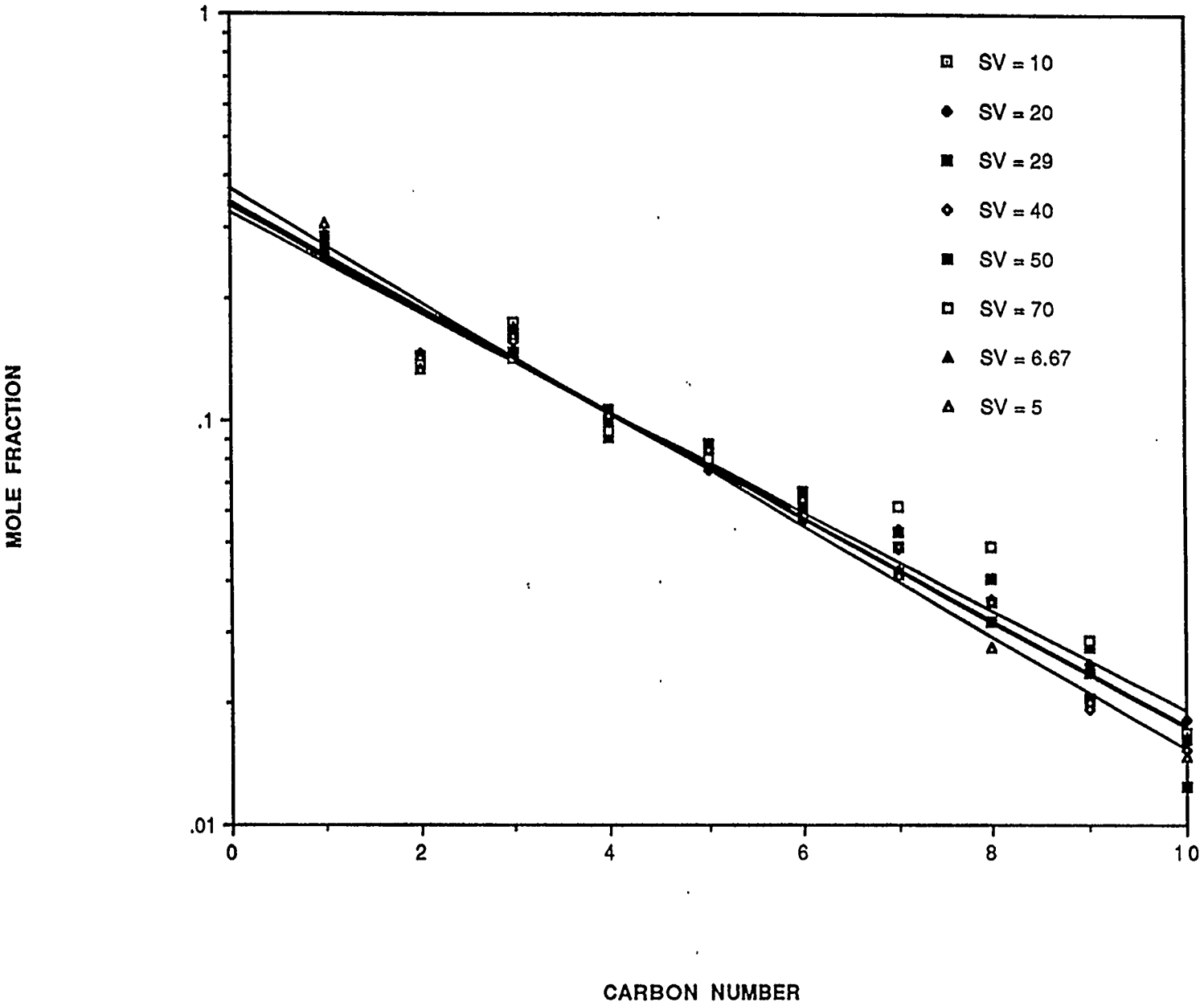

Figure 4.1.A.7 Rates of Fischer-Tropsch and Water Gas Shift Reactions

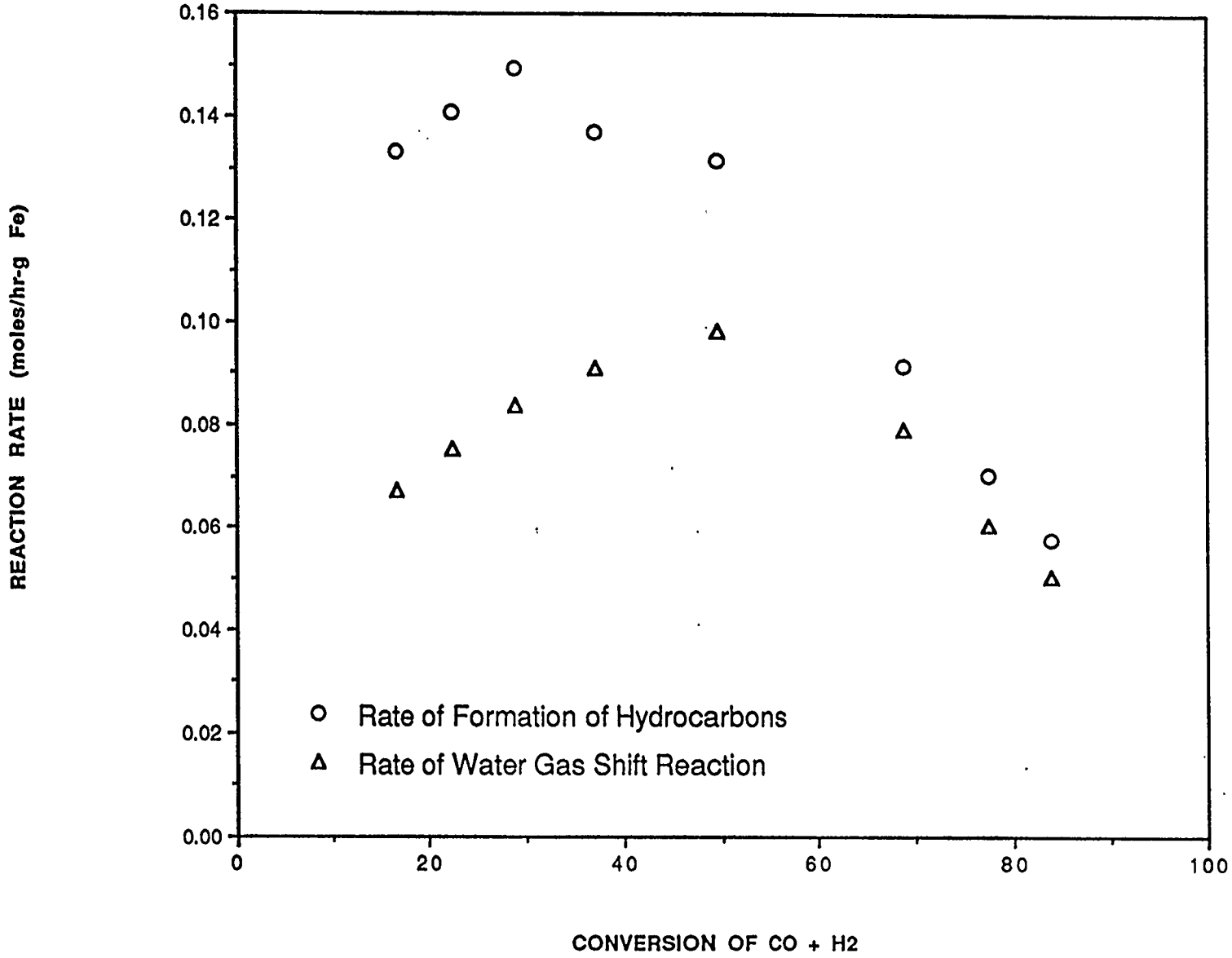

Figure 4.1.A.8 Fraction of CO converted to Hydrocarbons

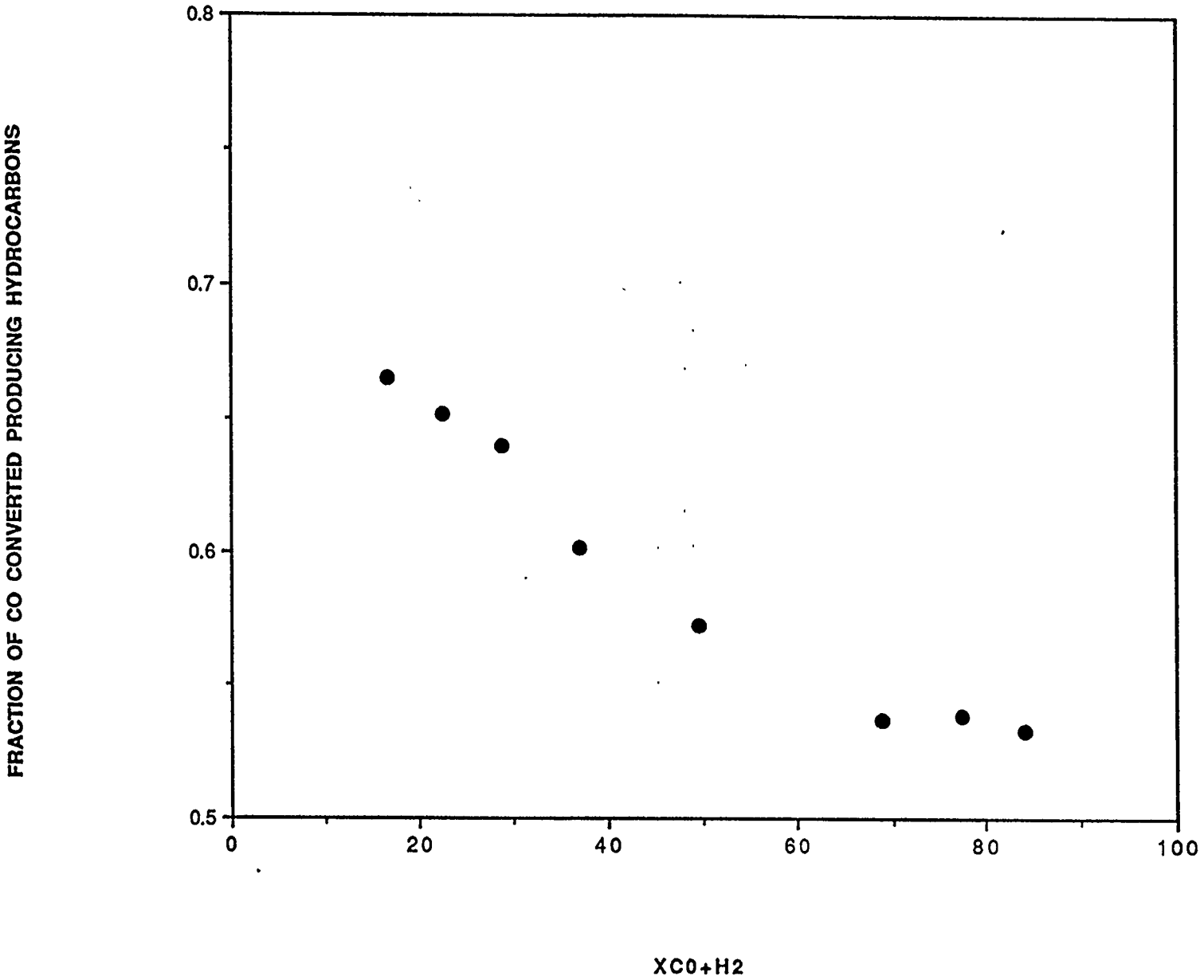

Figure 4.1.A.9 Test for Reaction Rate Expression (Eq. (6a))

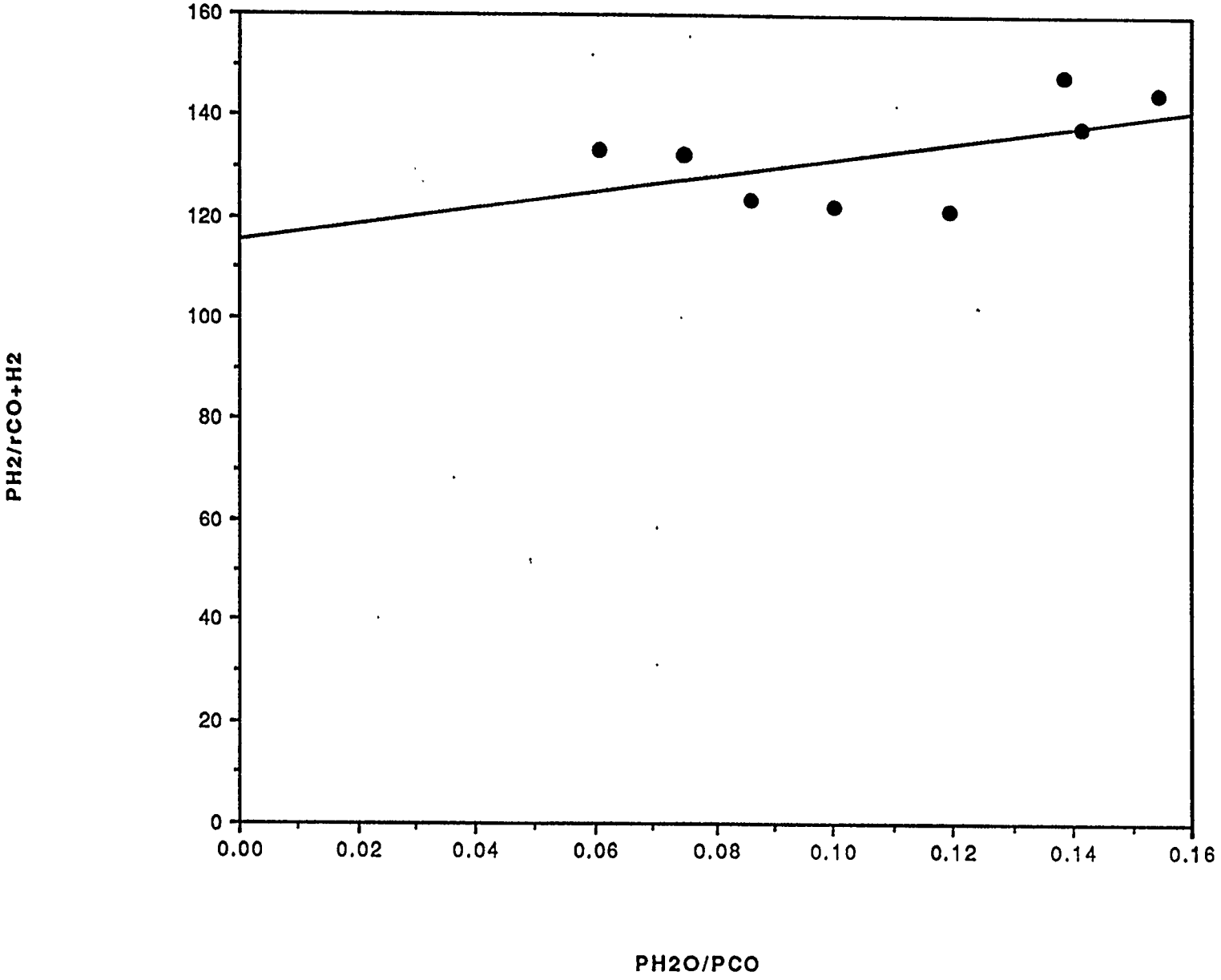

Figure 4.1.A.10 Test for Reaction Rate Expression (Eq. (6b))

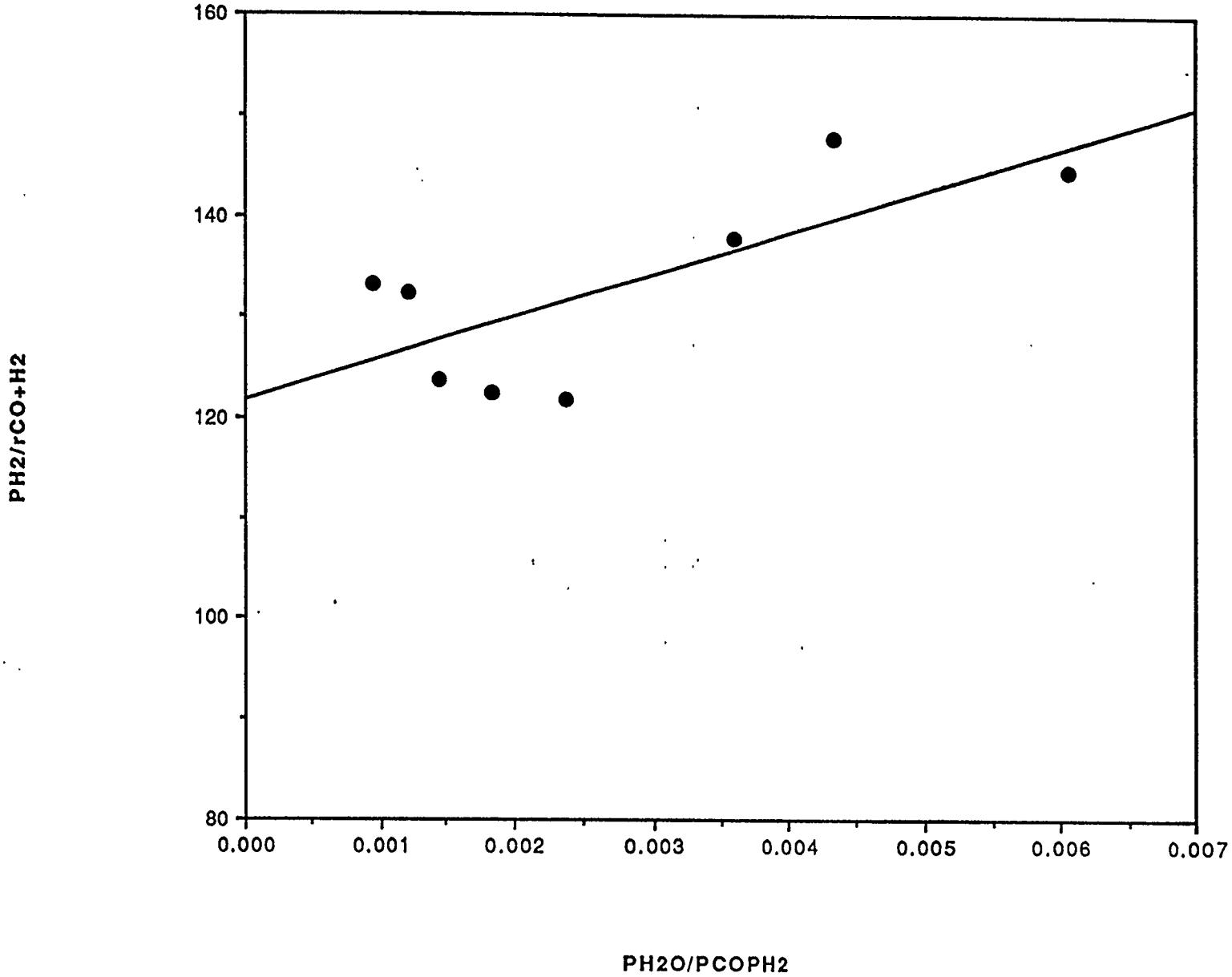

Figure 4.1.A.11 Test for Reaction Rate Expression (Eq. (6c))

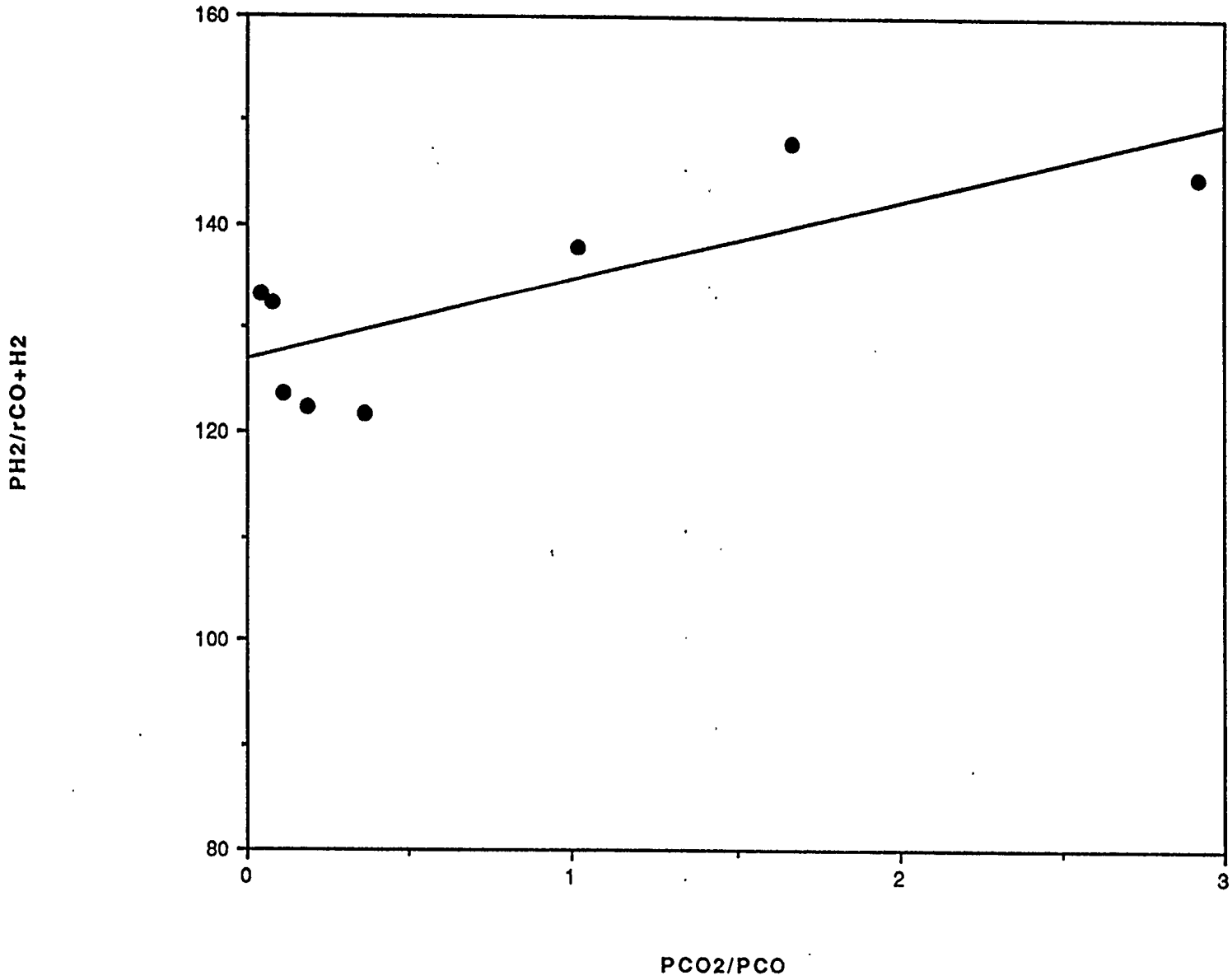

Figure 4.1.A.12 Test for Reaction Rate Expression (Eq. (7b))